On the Feasibility of Spray-Dried Eudragit-Trehalose Microparticles for Enteric Drug Delivery

Shabab Bin Karim[1], Mani Ordoubadi[1], Hui Wang[1], Mellissa Gomez[1], Reinhard Vehring[1]

[1]Department of Mechanical Engineering, University of Alberta, Edmonton, AB, Canada

Corresponding Author:

R. Vehring

University of Alberta

116 St & 85 Ave, Edmonton Canada

reinhard.vehring@ualberta.ca

Abstract

Enteric infections have long constituted a silent epidemic responsible for hundreds of thousands of deaths around the world every year. Because of the global rise in antibiotic-resistant bacteria and the slow development of new small-molecule antibiotics, alternatives such as bacteriophage therapy have become a much sought-after option in the treatment of enteric infections. However, the administration of therapeutics through the oral route to target gastrointestinal infections poses challenges to dosage formulation because these active ingredients, particularly relatively fragile biological entities, require protection from the stomach's harsh acids. Encapsulation of the therapeutics within a pH-responsive coating capable of surviving low pH conditions has the potential to provide such protection. In this study, we developed a spray-dried powder vehicle capable of withstanding low pH comparable to stomach conditions, using Eudragit® S100 as a protective particle coating and trehalose as a stabilizing excipient for a possible active component. A particle formation model and a monodisperse droplet chain

technique were initially used to study the formation process of Eudragit-trehalose composite microparticles at different ratios and in different ratios of water-ethanol solvent, which showed formation of particles with Eudragit shells varying in thickness from 0.13 µm to 0.75 µm. Promising Eudragit-trehalose formulations were subsequently spray-dried and their survival in acidic and alkaline environments studied using a new shadowgraphic imaging method. The results demonstrated that Eudragit was capable of creating a protective shell in the particles irrespective of the type of solvent used to prepare the formulations. The trehalose cores of particles with higher than 5% w/w of Eudragit remained protected after one hour of exposure at pH 2, indicating the potential of Eudragit-trehalose formulations for enteric delivery of drugs.

Keywords: Eudragit, enteric drug delivery, powder, pH-responsive dissolution, particle engineering, spray drying, shadowgraphic imaging

1. Introduction

Since their commercialization in the 1940s, antibiotics have been widely used to treat and prevent bacterial infections, but the emergence of antibiotic-resistant strains of various bacteria has become a serious global health threat. The World Health Organization has identified antimicrobial resistance as a growing public health threat of broad concern. Multidrug-resistance in *Mycobacterium tuberculosis* and malaria has been detected in multiple countries, and under-reporting of the cases compromises control efforts and jeopardizes recent advances (World Health Organization, 2014). *Escherichia coli, Salmonella* sp.*, Shigella* sp. and *Vibrio cholerae*, bacteria that are responsible for different gastrointestinal infections in humans and animals, have also shown alarming increases in their resistance to antibiotic use (Ashkenazi et al., 2003; Chiu et al., 2002; Glass et al., 1980; Mwansa et al., 2007; Reinthaler et al., 2003; Trung et al., 2005; van den Bogaard et al., 2001; Yoke-Kqueen et al., 2008). Since the development of new small-molecule antibiotics has failed to keep pace with the emergence of resistant strains of bacteria, alternative approaches are badly needed. Biologics, in particular bacteriophages, have the potential to fill the void and become a powerful tool in the treatment of antibiotic-resistant infections, including infectious enteritis.

Tablets are the most common means of delivering therapeutics to the enteric region in the treatment of enteritis. However, the tableting process involves a high degree of mechanical stress and the application of protective polymer layers at high temperatures for a prolonged period. Deliverable actives, especially biologics, require protection from stresses arising from manufacturing and storage conditions in order to maintain potency (Jończyk et al., 2011). In the

case of enteric delivery, both conventional pharmaceutical actives and bacteriophages require additional protection from the harsh chemical environment of the human stomach caused by the presence of hydrochloric acid and various digestive enzymes, as exposure to these substances can render them inactive (Abdelsattar et al., 2019; Koo et al., 2000; Koo et al., 2001).

Eudragit® is the commercial name for a range of polymethacrylate polymers marketed by Evonik Industries Inc. It is synthesized by the polymerization of acrylic acid and methacrylic acid or their esters at varying proportions (Rowe et al., 2009). Depending on their solubility profile, the different types of Eudragit can be divided into three broad classes (Thakral et al., 2013). Cationic Eudragit E, which is soluble below pH 5.5, is used as a film coating for taste-masking applications (Cerea et al., 2004; Drašković et al., 2017). Anionic Eudragit L and S, which are soluble above pH 6 and 7, respectively, have widespread application as enteric coatings for colon-specific drug delivery (El-Malah and Nazzal, 2008). Neutral Eudragit RL, RS (with pH-independent solubility) and NE, NM (with pH-dependent swelling and permeability) are used for sustained drug delivery (Das et al., 2010; Lunter and Daniels, 2012). Because of their ability to release drugs systematically at a targeted pH level, Eudragits are widely used as enteric coatings for tablets (Sauer et al., 2013). Historically, the coating process has employed conventional methods like dry powder coating (Sauer et al., 2013) and solvent evaporation (Perumal, 2001), both of which require heating the polymers for an extended period of time in order for them to coalesce and form the protective coating. When applied to biological dosage forms, any defect or inadequacy in this coating could cause biologics to be inactivated. The survival of biologics can also be threatened by the tablet-making process itself, which involves multiple compressing stages and considerable exposure to environmental and mechanical stress.

Spray drying is an alternative method of producing a dosage form that, unlike conventional multi-step coating processes, requires only a single step of droplet drying to form the protective outer shell of the particles. Spray drying is a process used to produce dry powder from a liquid feedstock, usually a solution or a suspension. The liquid feedstock containing dissolved or suspended solids is atomized into small droplets inside a drying chamber, and the droplets are then dispersed in a drying gas flow, where they evaporate and form particles. The dried particles are typically separated from the flow using a cyclone. Spray drying has been successfully applied in the food processing industry for the production of dried dairy and protein products and in taste-masking applications (Bora et al., 2008; Kim et al., 1996; Schuck, 2002). Spray drying is also often used in the pharmaceutical industry to encapsulate active ingredients within dried particles, a process that can provide protection from potentially hazardous environmental factors like high temperature and humidity (Carrigy and Vehring, 2019). Spray drying also allows for the design of particles with specific properties suitable for oral and respiratory delivery (Año et al., 2011; De Smet et al., 2014; Kunda et al., 2015; Saboo et al., 2016; Sou et al., 2015). Spray drying of Eudragit at laboratory scale to encapsulate different small molecule drugs for delivery into the gastrointestinal tract has been reported. Because of its insolubility in water, organic solvents like ethanol, methanol, dichloromethane, or mixtures of them, and aqueous suspensions or dispersions of Eudragit (Amiet-Charpentier et al., 1998) have been used to spray dry in conjunction with active pharmaceutical ingredients such as itraconazole (Sóti et al., 2015), diltiazem (Kristmundsdóttir et al., 1996), ketoprofen (Rassu et al., 2008), valsartan (Pradhan et al., 2016) and buspirone (Al-Zoubi et al., 2008).

The spray drying of biological actives like bacteriophages for pulmonary delivery has been successfully achieved in the past (Leung et al., 2018; Matinkhoo et al., 2011; Vandenheuvel et al., 2014). By comparison, studies on spray-dried powder formulations encapsulating biologics for enteric delivery are relatively scarce. In one reported study, an inactivated strain of *Vibrio cholerae* was spray-dried using an aqueous dispersion of Eudragit L 30D and FS 30D without any additional stabilizing agent. *In vitro* release studies showed that less than 5% of the encapsulated bacteria were released in an acidic medium, whereas 80% of the bacteria were released in a neutral medium over 24 hours (Año et al., 2011). A recent study focused on spray drying *Myoviridae* bacteriophage Felix O1 with Eudragit S100 and trehalose at different inlet temperatures (Vinner et al., 2019). Analysis of the produced powders showed a higher phage concentration in pure trehalose particles, but the survival of phages in simulated gastric fluid was much higher in particles containing Eudragit (Vinner et al., 2019). Despite these reported successes, few insights into the actual formation process of the particles, their specific core-shell morphology, and the underlying mechanisms for their ability to withstand exposure to the acidic pH of the stomach can be found in the published studies. A better understanding of the particle formation process is needed for a rational design of such particles.

In the present study solutions of Eudragit® S100 and trehalose were dried to explore the formation process of carrier particles with a polymer shell and a disaccharide core. Since Eudragit has high solubility in organic solvents and a pH-dependent solubility in water, two different feedstocks were prepared for drying with two different formulation approaches: an ethanol-water co-solvent system in which both Eudragit and trehalose had high solubility, and an aqueous system which dissolved both components by using a pH-shifting technique. The results of this

study shed light on previously unexplored details of the particle formation process of Eudragit-trehalose systems and the viability of spray-dried Eudragit-trehalose particles as a potential enteric delivery platform for small-molecule drugs and biologics, including bacteriophages, intended for gastrointestinal delivery in humans and animals.

2. Material and Methods

2.1. Chemicals and Formulations

Three different sets of feed solutions of trehalose dihydrate (Fisher Scientific Ottawa, ON, Canada) and poly (methacrylic acid-co-methyl methacrylate) (Eudragit® S100, Evonik Industries AG, Darmstadt, Germany) were prepared in different solvent compositions in this study. The first set of experiments assessed the influence of different ethanol (Commercial Alcohols, Winnipeg, Canada) and deionized water cosolvent ratios (0.6:0.4, 0.7:0.3, 0.75:0.25 and 0.76:0.24 [w/w]) on particle morphology. Feed solutions of trehalose and Eudragit with a fixed total solids concentration of 10 mg/mL were prepared at a 50:50 ratio. For the second set of formulations, feed solutions of trehalose and Eudragit were prepared using mixtures of ethanol and water at 0.76:0.24 (w/w), the iso-compositional point of the ethanol-water co-solvent system (Ordoubadi et al., 2019). Six formulations of trehalose/Eudragit were prepared with mass fractions of 0.50/0.50, 0.67/0.33, 0.80/0.20, 0.85/0.15, 0.90/0.10, and 0.95/0.05, keeping the total solids concentration fixed at 10 mg/mL. The third set consisted of different Eudragit-trehalose formulations spray-dried with water as the sole solvent. At neutral pH, Eudragit® S100 is insoluble in water. To make the water-based formulations, the pH of the water was initially shifted to the alkaline range (pH = 11) by adding 1M NaOH solution, which facilitated dissolution of the Eudragit

in the solvent. After the Eudragit had dissolved, the pH was readjusted to 7 by adding 0.01M HCl to neutralize the dissolved NaOH, since high alkalinity can be detrimental for biologics. Then, the necessary amount of trehalose was dissolved in the neutral solution. Six formulations with mass fractions of trehalose and Eudragit similar to formulations at the iso-compositional point were prepared in water. The pH of the formulations was monitored using a pH meter (Orion ROSS Ultra Semi-micro pH Electrode, Thermo Fisher Scientific, Waltham, MA, USA) at each step in the pH-shifting process.

2.2. Monodisperse Droplet Chain

A monodisperse droplet chain, an instrument capable of producing particles of nearly identical size, was used to gain insight into particle formation mechanisms and particle morphology. A simplified schematic is shown in Fig. 1; the details of the instrument are described elsewhere (Ordoubadi et al., 2019). Individual droplets of the feed solutions were dispensed inside a transparent, square tube using a piezoelectric droplet generator (Microfab Technologies Inc., Plano, Texas, USA) with a 40 µm orifice. Droplets were generated at a fixed frequency of 60 Hz. A laminar flow of air at 3 L/min was introduced at one end of the tube to dry the droplets, keeping the temperature at the inlet constant at 21 ˚C. The setup was improved for this study by using a laser interferometry technique to measure the initial droplet diameter more accurately at the inlet. A collimated laser beam (Process Instruments, Salt Lake City, Utah, USA) with a wavelength of 671 nm was passed through the stream of falling droplets at the inlet. A camera (GO-5000M-USB, JAI Inc., San Jose, CA, USA) placed at a fixed distance from the droplet chain was used to collect the angular phase function generated by the light scattered by the droplets. Captured phase functions were processed using MATLAB (MathWorks Inc., Natick, MA, USA) to determine

the average spacing between consecutive maxima of the angular scattering patterns. The initial droplet diameter was calculated using Eq. 1 (Hesselbacher et al., 1991),

$$d = \frac{2\lambda}{\Delta\theta_c}\left(\cos\left(\frac{\theta}{2}\right) + \frac{m\sin\left(\frac{\theta}{2}\right)}{\sqrt{m^2 - 2m\cos\left(\frac{\theta}{2}\right)+1}}\right)^{-1}, \quad (1)$$

where λ is the laser wavelength, $\Delta\theta_c$ is the angular spacing of the maxima in the angular scattering pattern, θ is the scattering angle, *m* is the refractive index of the droplet material, and *d* is the diameter of the droplet. In this study, the scattering angle was set at 43˚. Ethanol and water have similar refractive indices at room temperature (1.361 and 1.333); therefore, the change in refractive index of the solvent with varying proportions of ethanol and water was assumed to be insignificant. The refractive index of all the formulations was assumed to be equal to the refractive index of water at 25 ˚C. A schematic of the monodisperse droplet chain instrument and the methodologies for measuring the droplet diameter and capturing the dried particles are presented in Fig. 1.

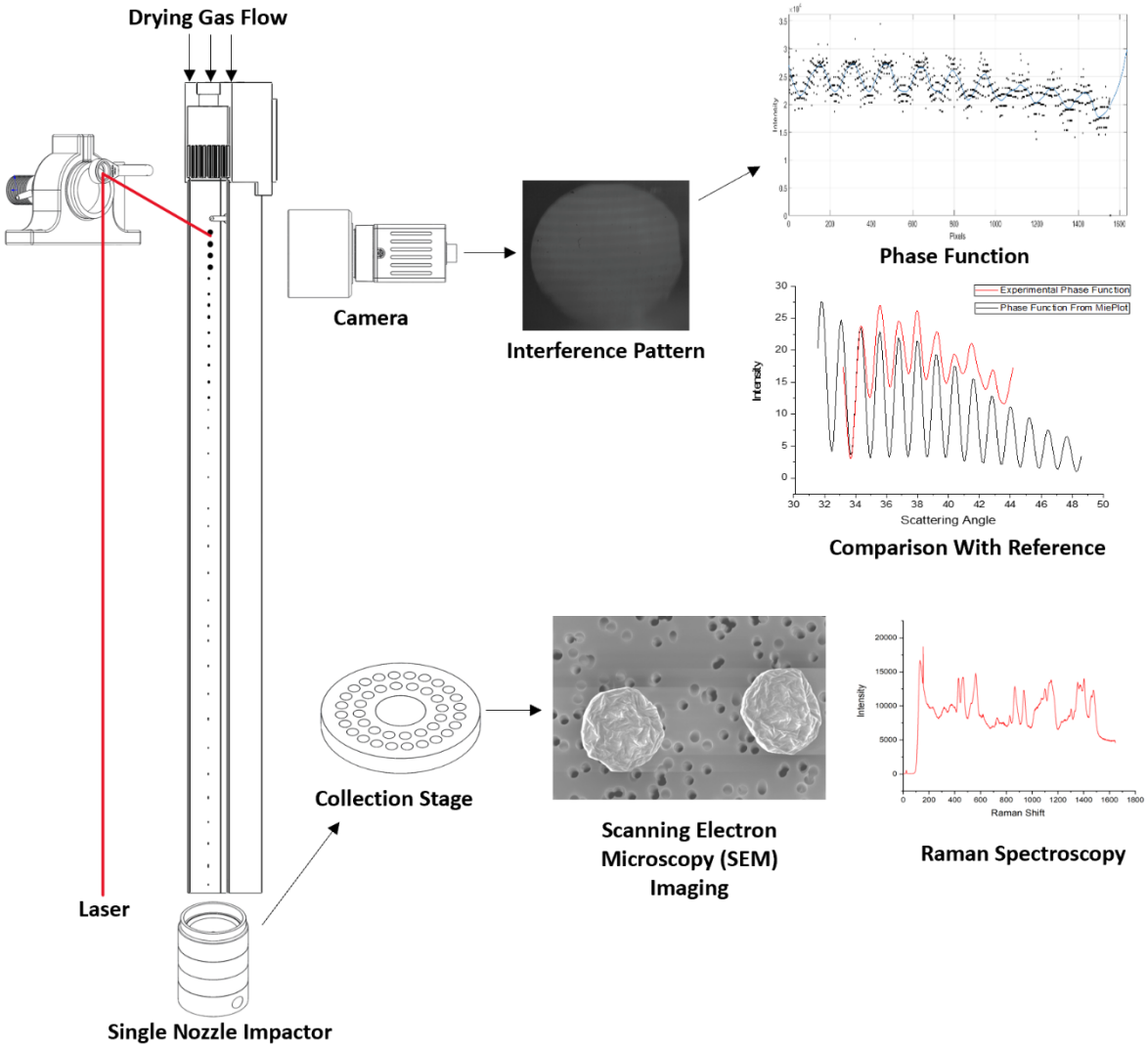

Fig. 1. Schematic of monodisperse droplet chain alongside the modifications made to the setup.

2.3. Polydisperse Spray Drying

Spray drying was used to produce larger batches of powder (2-3 g per batch) for dissolution analysis. Six feed solutions were prepared, each with a fixed total solute concentration of 20 mg/mL. Combinations of mass fractions of trehalose/Eudragit of 0.80/0.20, 0.85/0.15, 0.90/0.10, 0.95/0.05, 0.97/0.03 and 0.99/0.01 were dissolved in water by using the pH-shifting technique described in the previous section. A custom research spray dryer (Ivey et al., 2016) along with a

custom twin-fluid atomizer was used to spray-dry the formulations. The atomizer was operated at an air-to-liquid ratio of 20, defined as the ratio of air and liquid mass flow rates, which corresponded to an initial mass median droplet diameter of approximately 5.5 µm. The mass median diameter of the droplets was predicted using experimental data and methodology explained elsewhere (Hoe et al., 2014). The relevant spray drying parameters were calculated using a process model (Ivey and Vehring, 2010). The drying gas temperature was set to 100 ˚C for efficient drying of the droplets. The outlet temperature was limited to 58.4 ˚C to reduce thermal stress at the outlet of the cyclone. Similarly, outlet humidity was limited to 3.4% RH to prevent crystallization of the powder during collection. The feedstocks were supplied to the atomizer using a peristaltic pump (Cole-Parmer, Montreal, QC, Canada) at 1.7 mL/min, with a fixed drying gas flow rate of 400 SLPM. The collected powders were bottled in airtight glass vials and stored under dry conditions at ambient temperature for subsequent analysis. The morphology of the spray-dried particles was examined using scanning electron microscopy.

2.4. Computation of Particle Formation Parameters

Particle formation in a co-solvent system with two solutes is a complex process. As multiple solvents evaporate, the dissolved solutes are precipitated sequentially according to their solubility, solid phase, density, and diffusivity, leaving behind the solid particles. To understand the particle formation process in the studied co-solvent systems, a numerical model for multi-solvent microdroplet evaporation first described by Ordoubadi et al. (2019) was used. The internal distribution of solutes in the evaporating droplets dictates the morphology of the dried particles (Boraey and Vehring, 2014; Vehring et al., 2007). This distribution depends on both the rate of evaporation of the droplet over time, and the rate of diffusion of the solutes inside the

droplet. The effect of these counteracting mechanisms can be expressed by the Péclet Number, which is defined as the ratio of evaporation rate to the diffusion coefficient of each component, $D_{i,}$ as shown below (Vehring, 2008):

$$Pe_i = \frac{\kappa}{8D_i}. \qquad 2$$

The evaporation rate, κ, which describes the instantaneous rate of shrinkage of the droplet surface area, was calculated from the numerical model for the multi-solvent systems studied here. This instantaneous evaporation rate was obtained from the calculated droplet surface areas at two consecutive time steps. The details of the numerical model used can be found elsewhere (Ordoubadi et al., 2019). For small Péclet numbers, the diffusional motion of the solute molecule within an evaporating droplet, i, is relatively fast compared to the recession speed of the droplet surface. This ensures uniform distribution of the solute throughout the droplet, resulting in solid, spherical particles, provided that the solutes are not surface-active and do not have low solubility (Ordoubadi et al., 2021b). Large Péclet numbers of solute molecules, as in the case of polymers like Eudragit, are caused by their large size, which restricts the movement of the molecules within the droplet and slows diffusion compared to the recession of the droplet surface. As a result, the solute enriches near the surface of the droplet and typically forms particles with hollow centers and shells.

The Einstein-Stokes equation was used to approximate the diffusion coefficient of the components in a single solvent based on molecular size. Assuming spherical molecules, the molecular radius of Eudragit was approximated from its bulk density data to be 3.15 nm. The molecular radius of trehalose, obtained from its molecular volume (Edward, 1970), was

calculated to be 0.41 nm. To approximate the diffusion coefficient of each solute in a well-mixed co-solvent system, a mass-weighted average of the binary diffusivities in different solvents was considered. This assumption does not provide an accurate molecular diameter of the polymer; however, this simple approximation is suitable for predicting the Péclet number of the large polymer molecule (125 kDa), which is almost an order of magnitude higher than that of trehalose.

Due to surface enrichment, the component with a higher Péclet number will typically solidify first near the droplet surface, whereas the component with a lower Péclet number will solidify throughout the droplet, including the core, at a later stage. In a co-solvent system with a highly volatile component, such as ethanol, the evaporation rate and the diffusion coefficients do not remain constant over time, resulting in a time-varying Péclet number (Ordoubadi et al., 2019). Therefore, in this study, the internal solute profiles during drying were predicted through a numerical solution of the internal mass transfer equation as explained elsewhere (Ordoubadi et al., 2019).

The shell thickness is a critical parameter for assessing how well the core of a particle will be protected within an acidic environment. For droplets containing high Péclet number solutes, the shell thickness of the dried particles can also be approximated using particle formation theory (Boraey and Vehring, 2014). At the predicted instance of shell formation, the droplet diameter is considered to equal the volume-equivalent diameter of the particle, assuming that the remaining solvent in the interior evaporates through the shell without causing further shrinkage. The remaining solutes in the interior of the droplet will increase the shell thickness due to mass flux towards the interior of the wall during continuing evaporation. Assuming that all of the solute

mass concentrates as a thin shell at the end of the evaporation process, and estimating the average shell density, ρ_{sh}, from the true density of the solute, the internal particle diameter, d_{sh}, can be expressed as (Boraey and Vehring, 2014)

$$d_{\mathrm{sh}} = d_{\mathrm{v}}\left(\sqrt[3]{1-\frac{\rho_{\mathrm{p}}}{\rho_{\mathrm{sh}}}}\right), \quad 3$$

where d_{v} is the volume equivalent diameter of the particle and ρ_{p} is the calculated particle density, which can in turn be expressed as

$$\rho_{\mathrm{P}} = C_{\mathrm{f}}\left(\frac{d_0}{d_{\mathrm{v}}}\right)^3, \quad 4$$

where C_{f} is the total solids feed concentration. For a multi-component system, the true density of the shell, ρ_{sh} can be estimated using Eq. 5,

$$\rho_{\mathrm{sh}} = \frac{1}{\sum_i \frac{Y_i}{\rho_i}}, \quad 5$$

where ρ_i and Y_i are the true density and mass fraction of the component i. The shell thickness of the particle, l_{sh}can then be represented as

$$l_{\mathrm{sh}} = \frac{d_{\mathrm{v}} - d_{\mathrm{sh}}}{2}, \quad 6$$

where d_{v} is the volume-equivalent diameter of the particle at the onset of shell formation at the surface.

Using the calculated surface enrichment results, it is possible to approximate the time required for the solute surface concentration to reach true density and form the shell of the particle in the

case of a constant evaporation rate. The time at which co-solidification of a multi-component amorphous mixture occurs , $t_{t,mix}$, is defined as (Carrigy et al., 2019)

$$t_{\mathrm{t,mix}} = \tau_{\mathrm{D}} \left[1 - \left(\sum_i E_i \frac{C_{0,i}}{\rho_{\mathrm{t},i}} \right)^{\frac{2}{3}} \right], \quad (7)$$

where $C_{0,i}$, is the initial solids concentration of component i, $\rho_{\mathrm{t},i}$ is the true density of component i, and $\tau_{\mathrm{D}} = \frac{d_0^2}{\kappa}$ is the droplet lifetime.

The model assumes co-solidification to occur after the mixture reaches true density at the surface. For the calculation, the true densities of trehalose and Eudragit S100 were 1580 kg/m^{-3} (Grasmeijer et al., 2016) and 841 kg/m^{-3} (Evonik Industries, 2012), respectively.

The model was also used to estimate the particle density using the calculated volume-equivalent diameter of the particles and the true density of the mixture as calculated by Eq. 5.

The particle morphology can then be predicted using the ratio of particle density and true density of the mixture (Carrigy et al., 2020). If this value is considerably smaller than 1, the particles are expected to be hollow, which may lead to buckled or wrinkled morphologies because the shells may lack mechanical strength to maintain spherical shape; the particles are also expected to have a smaller diameter than the predicted value. For values closer to 1, the particles are expected to be solid and spherical in shape.

2.5. Field Emission Scanning Electron Microscopy

Particles obtained from the monodisperse droplet generator technique and spray drying were analyzed for morphological differences based on formulation differences. The dried particles produced by the monodisperse droplet generator were collected at ambient conditions using a single-nozzle impactor (Wang et al., 2017b). This custom impactor consists of several removable stages with different cutoff diameters ranging from 21 µm to 0.6 µm. Based on the predicted particle diameter, the impactor was configured with two suitable stages. The outlet of the impactor was connected to a vacuum pump which provided an air flow of 3 L/min. The dried particles impacted directly onto the surface of removable aluminum SEM pin mounts (Ted Pella, Inc.; Redding, CA, USA) covered by carbon tape, which were used for scanning electron microscopy imaging without further sample transfer. Particles produced by spray drying were manually transferred from a collection bottle to the carbon tape-covered surfaces of the aluminum mounts within a dry environment. Prior to imaging, the samples were coated with a mixture of 80% gold and 20% palladium to a thickness of approximately 10-15 nm using a sputter coater (Leica ACE600 Carbon/Metal Coater; Concord, ON, Canada). The particles were imaged by a field emission scanning electron microscope (Zeiss Sigma FESEM, Oberkochen, Germany) with an immersion lens (in-lens) detector operated at an accelerating voltage of 3.00 to 5.00 kV and using magnifications of 1000x to 5000x at a working distance of 5 mm to 6 mm.

2.6. Dissolution Test using Shadowgraphic Imaging Technique

A new shadowgraphic imaging method and associated instrument were used to analyze the dissolution rate of the spray-dried powders in two solutions at different pH. 300 mg of each

295 spray-dried powder was added to 20 mL of 0.01M hydrochloric acid (pH = 2.0) and 1μM of sodium hydroxide solution (pH = 8) separately in glass vials. The suspensions were stirred with a magnetic stirrer for extended periods of time (one hour for HCl, two hours for NaOH). The imaging instrument (Wang et al., 2018) consisted of a high-resolution camera (SP-5000M-PMCL, JAI Inc., San Jose, CA, USA), fitted with a 16mm fixed-focal length lens (Edmund Optics Inc., NJ, USA),
300 which took sequential shadowgraphic images of the liquid samples. A collimated LED backlight (Advanced Illumination Inc., Rochester, VT, USA), which was connected to a high-output strobe controller (Pulsar 320, Advanced Illumination Inc., Rochester, VT, USA) and a two-channel function generator (AFG1022, Tektronix Inc., Beaverton, OR, USA) that synchronized the camera and the LED backlight, was used to illuminate the glass vial containing the suspension in a bright
305 field. To avoid interference from external light sources, all optical components were enclosed in a light-blocking sample chamber. The interior of the chamber was covered with light-absorbing material in order to minimize interference by reflected light rays. The acquired images were processed to obtain the normalized relative transmission intensity, $\Delta T_{t,h}^{\mathrm{N}}$, and the transmission coefficient, $\sigma(t)$, as a function of time. Normalized relative transmission intensity was calculated
310 using the following equation (Wang et al., 2018),

$$\Delta T_{t,h}^{\mathrm{N}} = \frac{\Delta T_{t,h}}{\Delta T_{\mathrm{Clear}}^{\mathrm{a}} - \Delta T_{t_0,h}^{\mathrm{a}}}, \tag{8}$$

where $\Delta T_{t,h}$ is the measured relative transmission, $\Delta T_{\mathrm{Clear}}^{\mathrm{a}}$ is the transmission through a clear control medium and $\Delta T_{t_0,h}^{\mathrm{a}}$ is the initial transmission through the sample.

The transmission coefficient is the integral of the normalized relative transmission intensity over the sample height, *h*, and indicates the overall change in transmission intensity over time as a dimensionless number ranging from 0 to 1.

$$\sigma(t) = \int_{h=0}^{h=1} |\Delta T_{t,h}^{\mathrm{N}}| \, . \qquad 9$$

OriginLab (Northampton, MA, USA) was used to perform regression on the transmission coefficient curves.

In cases where a sample is insoluble in a given medium, the transmission of light through the suspension will remain unchanged, resulting in a constant transmission coefficient. By contrast, when a sample slowly dissolves in a given medium, the corresponding coefficient increases with the transmission of light through the suspension. Although the associated setup is used for measuring colloidal stability of suspensions, the introduction of a stirrer canceled the effect of particle sedimentation and creaming, thus attributing the change in transmission coefficient to the change in suspension concentration. The change in transmission coefficient can also be attributed to other factors, such as changes in particle size or the refractive indices of the particles or the fluid. The suspension concentration has an inverse relationship with the transmission coefficient, since relative transmission of light through the glass vials, and consequently the transmission coefficient, increases as the suspension concentration decreases. However, due to the influence of the other factors mentioned, this technique is semi-quantitative. For more in-depth evaluation of the dissolution rate in vivo, methods similar to the one described by (Serrano et al., 2016) would be more suitable.

2.7. Raman Spectroscopy

To evaluate the protection of trehalose provided by a Eudragit coating in the acidic environment, a solid-phase analysis of the residual mass was conducted using a custom-designed dispersive Raman spectroscopy system (Wang et al., 2017a). All suspension samples in the acidic medium were filtered after the dissolution test. The residual sludges for all cases in which the suspended particles did not dissolve completely were washed with deionized water and further filtered and dried in a vacuum chamber. Samples were loaded in the conical cavity of a rectangular metallic slide and then placed in an enclosed signal-collection chamber. The Raman setup used a 670 nm diode-pumped solid-state laser. A continuously variable neutral-density filter was used to control the laser beam power, while a cryogenically cooled CCD sensor array was used to collect the signal. All the resulting Raman spectra were measured at temperatures of 20 to 22 ˚C and at less than 2% RH. The spectra of the samples were deconvoluted for quantification of amorphous and crystalline components using methods explained elsewhere (Vehring, 2005).

3. Results and Discussion

3.1. Particle Formation in Cosolvent Systems

3.1.1. Effect of Cosolvent Ratio on Particle Formation

To apply the particle formation model, it is first necessary to determine the evaporation rate (cf. Eq. 2) for the different solvent systems used in this study. The droplet surface area normalized by the initial droplet surface area as a function of time was determined for different ethanol contents and plotted in Fig. 2. The slopes of the plots are the evaporation rates. To allow for direct comparison, the time axis was normalized by the square of the initial diameter, which is

proportional to the time it takes droplets with the same evaporation rate to evaporate completely. It is apparent that the evaporation rate is a function of solvent composition and is not constant throughout the life of the droplets for most compositions. At a higher water content, the evaporation rate decreases, indicating a change in composition over time. However, as the solvent composition approaches the isocompositional point of the water-ethanol mixture, the evaporation rate becomes constant. The isocompositional point of an evaporating multicomponent droplet at ambient temperature, relative humidity and pressure is the compositional point at which the mass fractions of the components, the temperature, and the composition-related properties, such as the evaporation rate, Péclet number, droplet temperature, solute solubilities etc., remain constant for the majority of the droplet's lifetime (Ordoubadi et al., 2019).

The multi-solvent microdroplet evaporation model also provided the average solvent composition as a function of time. Because of a lack of experimental literature data, the solubility of Eudragit at different water-ethanol co-solvent ratios was calculated using a log-linear approximation. Both solubility and ethanol mass fraction are plotted as a function of time in Fig. 3. It is apparent that the solubility of Eudragit at any given point in time strongly depends on the mass fraction of ethanol remaining in the droplet. Formulations with decreasing ethanol content showed a rapid drop in the solubility of Eudragit as the mass fraction of ethanol decreased. However, for the composition at the isocompositional point, the solubility of Eudragit in the solvent was relatively high and stayed constant until the end of the drying process. During the drying process very close to the isocompositional point, the water can evaporate completely near the end of the evaporation process, causing the ethanol fraction of the droplets to rise rapidly.

This increase in turn results in a rapid increase in the solubility of Eudragit within the droplets, as seen in the last system in Fig. 3.

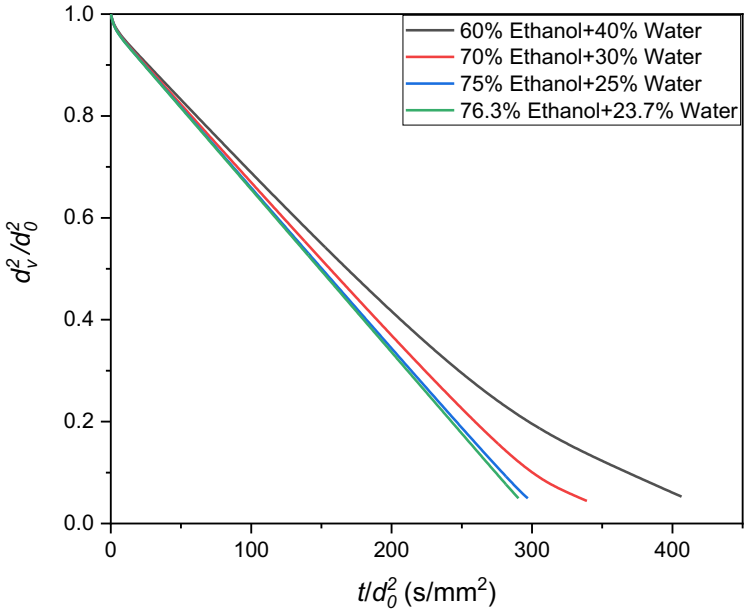

Fig. 2. The normalized surface area of ethanol-water droplets at different compositions evaporating at 21 ˚C as a function of normalized time, as predicted by a numerical model. The slope of the curves is a measure of the evaporation rate.

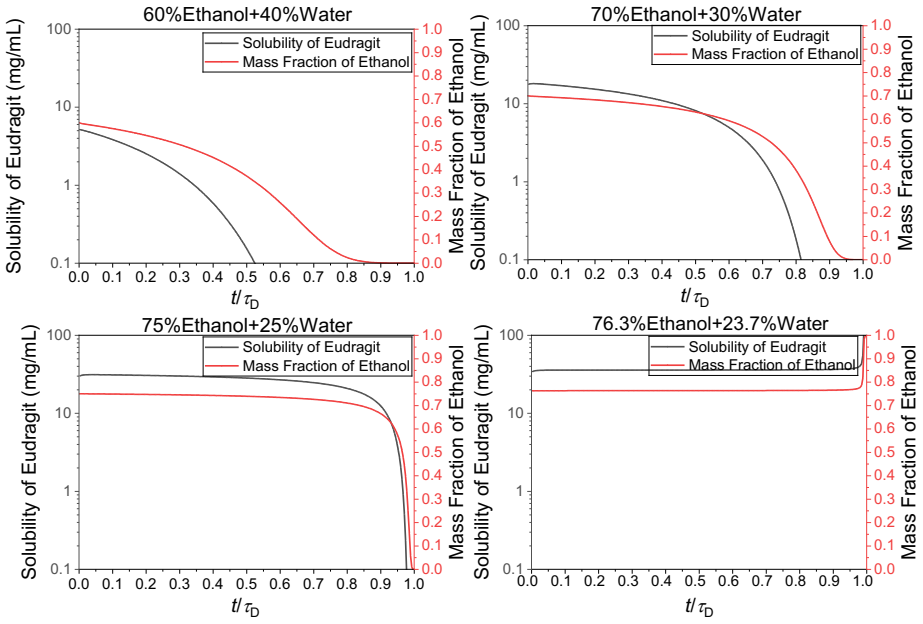

Fig. 3. The effect of ethanol mass fraction in the co-solvent (red lines and right axis) on the solubility of Eudragit (black lines and left axis) as predicted by a numerical model, shown as a function of time for the evaporating droplets, normalized by the droplet lifetime.

The concentration of Eudragit on the surface of the droplet was modelled to predict the onset of shell formation. Fig. 4 shows the Eudragit surface enrichment, i.e., the surface concentration normalized by the average concentration, as a function of normalized time for different co-solvent compositions. A higher surface enrichment is desirable for the formation of a core-shell structure. However, the surface enrichment at the lower ethanol content showed a reduction in the later phases of evaporation, where the co-solvent composition shifted towards water and the evaporation rate decreased. This is because surface enrichment is a direct function of the Péclet number and feedstocks with lower ethanol content will lead to water-enriched droplets in the later phases of droplet drying. Despite the low solubility of Eudragit in water, the much slower evaporation rate of water than of ethanol is primarily responsible for the reduced surface

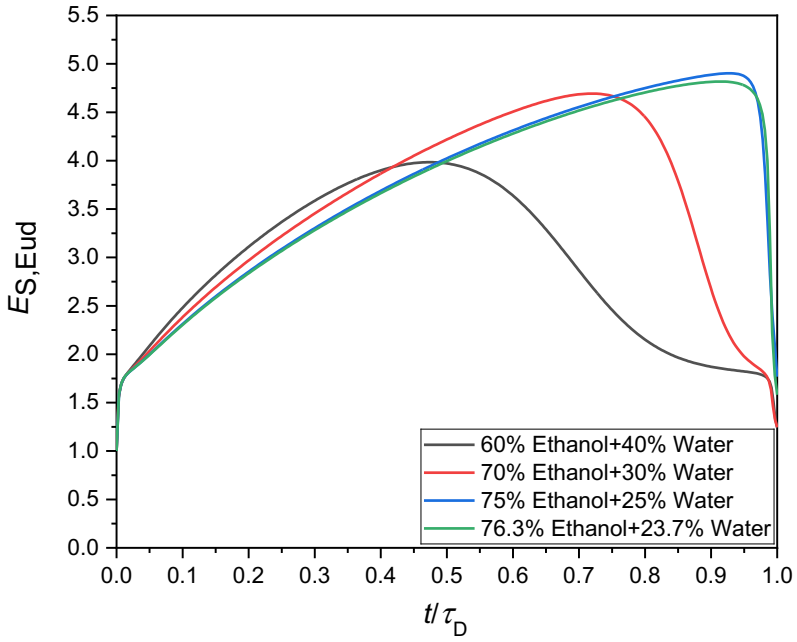

Fig. 4. Surface enrichment of Eudragit at different solvent compositions as predicted by a numerical model. Surface enrichment was a function of the Péclet number at any given time. The change became steady and reached a peak at the iso-compositional point of the water-ethanol mixture.

enrichment. At or near the iso-compositional point the Péclet number remained steady, resulting in a continuous increase in surface enrichment over time towards the maximum value. For proper coating of particles, a higher surface enrichment of Eudragit is desirable, which in turn requires a solvent prepared close to the iso-compositional point of ethanol-water mixture.

Table 1 shows various parameters related to shell formation that were calculated using the particle formation model for a Eudragit-trehalose binary system at a ratio of 50:50 dried in the monodisperse droplet chain. For these calculations it was assumed that Eudragit remained amorphous and commenced shell formation when the true density of the mixture was reached

395 at the surface. All the formulations took more than 90% of droplet lifetime to reach their true density, a consequence of the low initial feed concentration. The particle density was calculated according to Eq. 4. The results predicted low density particles, especially for the co-solvent ratios at or near the iso-compositional point. The true density of the mixture of Eudragit and trehalose was estimated with Eq. 5 using the predicted mass fractions of the components at the surface at 400 the time when true density was reached. The normalized $\rho_{\mathrm{P}}/\rho_{\mathrm{t,mix}}$ values predicted the particles to be hollow and likely wrinkled. The shell thickness was approximated using Equation 6. It decreased slightly with increasing ethanol content in the formulations.

Table 1 Results of the particle formation modeling for parameters related to shell formation for different solvent compositions and a Eudragit-trehalose ratio of 50:50. Shown are time to reach 405 true density ($t_{\mathrm{t,mix}}$) on the surface, normalized by the droplet life time ($t_{\mathrm{t,mix}}/\tau_{\mathrm{D}}$); predicted particle density (ρ_{P}); true density of the excipient mixture ($\rho_{\mathrm{t,mix}}$); normalized particle density ($\rho_{\mathrm{P}}/\rho_{\mathrm{t,mix}}$); and estimated shell thickness of the particles.

Solvent Composition		$\boldsymbol{\frac{t_{\mathrm{t,mix}}}{\tau_{\mathrm{D}}}}$	$\boldsymbol{\rho_{\mathrm{P}}}$ **(kg m^{-3})**	$\boldsymbol{\rho_{t,\mathrm{mix}}}$ **(kg m^{-3})**	$\boldsymbol{\rho_{\mathrm{P}}/\rho_{\mathrm{t,mix}}}$	**Shell Thickness (μm)**
Ethanol (%)	**Water (%)**					
60	40	0.99	700	1020	0.70	0.75
70	30	0.95	650	1000	0.65	0.60
75	25	0.91	300	940	0.32	0.50
76.3	23.7	0.92	300	940	0.32	0.50

Fig. 5 shows the scanning electron microscopy images of the particles collected from the monodisperse droplet chain experiments corresponding to the cases listed in Table 1. The monodisperse droplet chain instrument was operated at a significantly lower temperature (21˚C) than the spray dryer (100˚C). The objective in using a monodisperse droplet chain was to obtain a preliminary idea of the particle formation process for the binary trehalose-Eudragit system at different solvent compositions. Upon drying, trehalose forms fairly smooth spherical particles. The addition of Eudragit to the formulations visibly changed the particle morphology as Eudragit enriched the particle surface. Although the particles are not spherical, they appear to be monodispersed, with consistent morphology. In all cases, the particles show a similarly folded structure with low particle density due to external void space, as predicted by the values of $\rho_{\mathrm{P}}/\rho_{\mathrm{t,mix}}$ in Table 1. In all considered solvent compositions, the Péclet number of Eudragit was much larger than that of trehalose. As a result, Eudragit preferentially accumulated on the surface of the droplets and subsequently formed large, hollow particles with a thin shell, as predicted. Assuming that the fold thickness of the particles in the SEMS was about twice the shell thickness, the shell thickness was estimated to be between 500 and 650 nm, a good agreement with the predictions reported in Table 1. The SEMs also reveal a visible increase in the projected particle area with increased ethanol content, demonstrating earlier shell formation and thinner shell thickness.

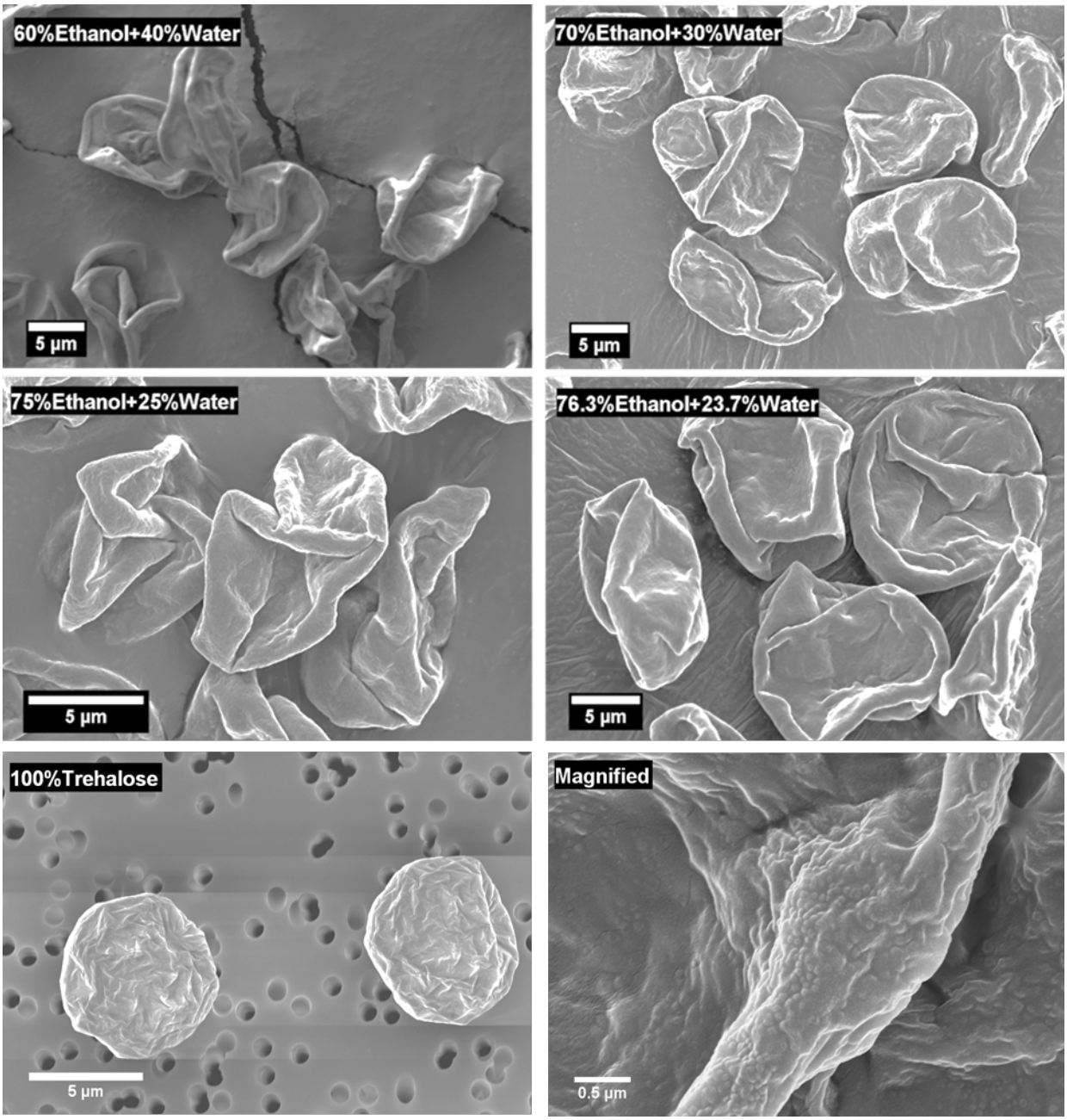

Fig. 5. Scanning electron microscopy (SEM) images of particles collected from the monodisperse droplet chain dried at a gas temperature of 21 ˚C. The solvent compositions were changed keeping the total excipient concentration constant at 5 mg/mL each of Eudragit and trehalose. The external morphology showed hollow, extremely folded particles for all four solvent compositions. Comparison of the SEMs to solid spherical trehalose particles suggests the presence of Eudragit at the surface of the particles. The SEM at the bottom right corner shows a magnified image of a microparticle indicating the thickness of the shell at the fold. Scale bars are shown separately for each image.

A particle with sufficient protection against a low pH environment must have a shell that consists primarily of Eudragit rather than trehalose. Shell composition can be predicted by modelling the concentration of the excipients as a function of radial coordinate in the droplets. Fig. 6 shows the radial profiles of the mass fractions of Eudragit and trehalose within the particles at the time when shell formation is predicted to begin, calculated using the particle formation model. The radial coordinate *r* was normalized by the droplet radius, *R*. It is apparent from the figure that the highest concentrations of Eudragit at the surface were achieved with the formulation at or near the iso-compositional point. This finding indicates that this co-solvent composition is beneficial for protecting the core of the particles with Eudragit.

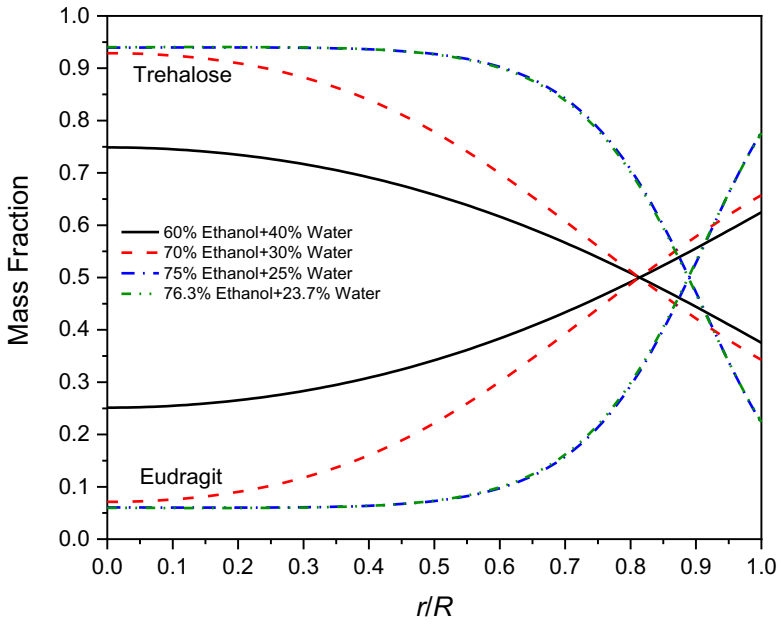

Fig. 6. Radial distribution of components within the evaporating droplets for different solvent compositions at the time shell formation is predicted to commence. More Eudragit reached the surface at higher Ethanol compositions because of higher surface enrichment.

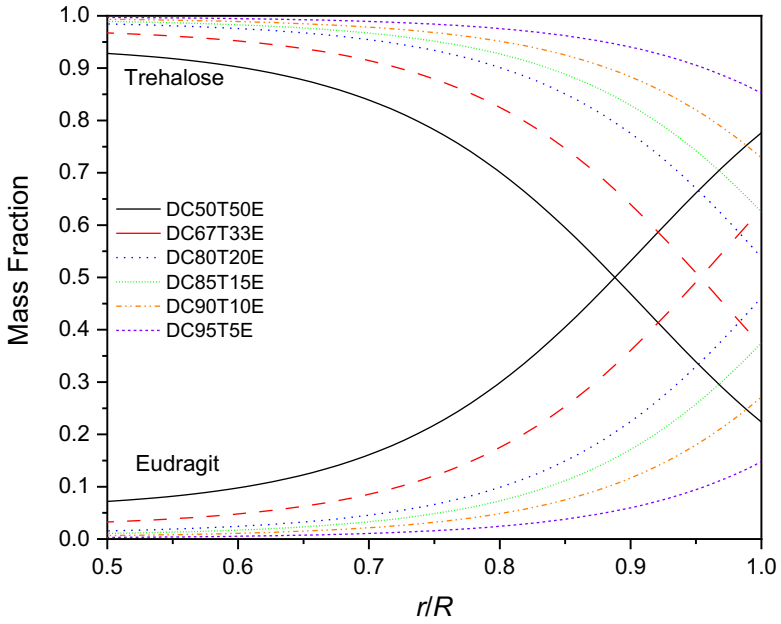

Fig. 7. Radial distribution of components within the evaporating droplets in an ethanol-water co-solvent at the iso-compositional point. Particles with higher Eudragit content had more polymer at the surface.

3.1.2. Effect of Excipient Mass Fraction on Particle Formation

The next question that needs to be addressed is how much Eudragit in the formulation is required for the formation of a protective shell. Calculations for particle formation at the iso-compositional point for varying ratios of trehalose and Eudragit provide a deeper insight into the effect of the excipient ratio on the particle morphology. The radial distribution of the excipients within the droplets was calculated at the time the surface concentration was predicted to reach the true density of the mixture. The results as a function of normalized radius are shown for the outer regions of the droplet ($r/R > 0.5$) in Fig. 7. With increasing trehalose fractions the Eudragit

concentration at the surface gradually decreased. For the three formulations with the lowest Eudragit fraction up to 15%, trehalose remained the predominant component on the surface, a situation unlikely to lead to the formation of a Eudragit shell.

The calculations presented in Table 2 also predicted a gradually decreasing shell thickness with decreasing Eudragit fractions in the particles. Normalized particle density values, $\rho_{\mathrm{P}}/\rho_{\mathrm{t,mix}}$, predicted the particles would become more spherical and solid with decreasing Eudragit content. All of these findings are consistent with the morphology of the particles as illustrated by the SEM images shown in Fig. 8. For the case studied here, a Eudragit mass fraction of less than 15% did not lead to the desired core-shell morphology. However, this is true only for the low drying gas temperature of 21 °C used in the droplet chain apparatus; spray dryers typically use much higher drying gas temperatures.

Table 2 Results of the particle formation modeling for parameters related to shell formation for different Eudragit-trehalose ratios at the iso-compositional composition of ethanol-water. Shown are time to reach true density ($t_{t,mix}$) on the surface, normalized by the droplet lifetime, ($t_{t,mix}/\tau_D$); predicted particle density (ρ_P); true density of the excipient mixture ($\rho_{t,mix}$); normalized particle density ($\rho_P/\rho_{t,mix}$); and estimated shell thickness of the particles collected from the monodisperse droplet chain at 21 ˚C.

Formulation	$\frac{t_{\mathrm{t,mix}}}{\tau_{\mathrm{D}}}$	ρ_{P} (kg m^{-3})	$\rho_{t,\mathrm{mix}}$ (kg m^{-3})	$\rho_{\mathrm{P}}/\rho_{\mathrm{t,mix}}$	**Shell Thickness (µm)**
DC50T50E	0.93	310	940	0.33	0.65
DC67T33E	0.94	410	1020	0.40	0.50
DC80T20E	0.95	560	1120	0.5	0.49

DC85T15E	0.96	660	1190	0.55	0.50
DC90T10E	0.97	760	1280	0.59	0.38
DC95T5E	0.97	960	1400	0.69	0.20

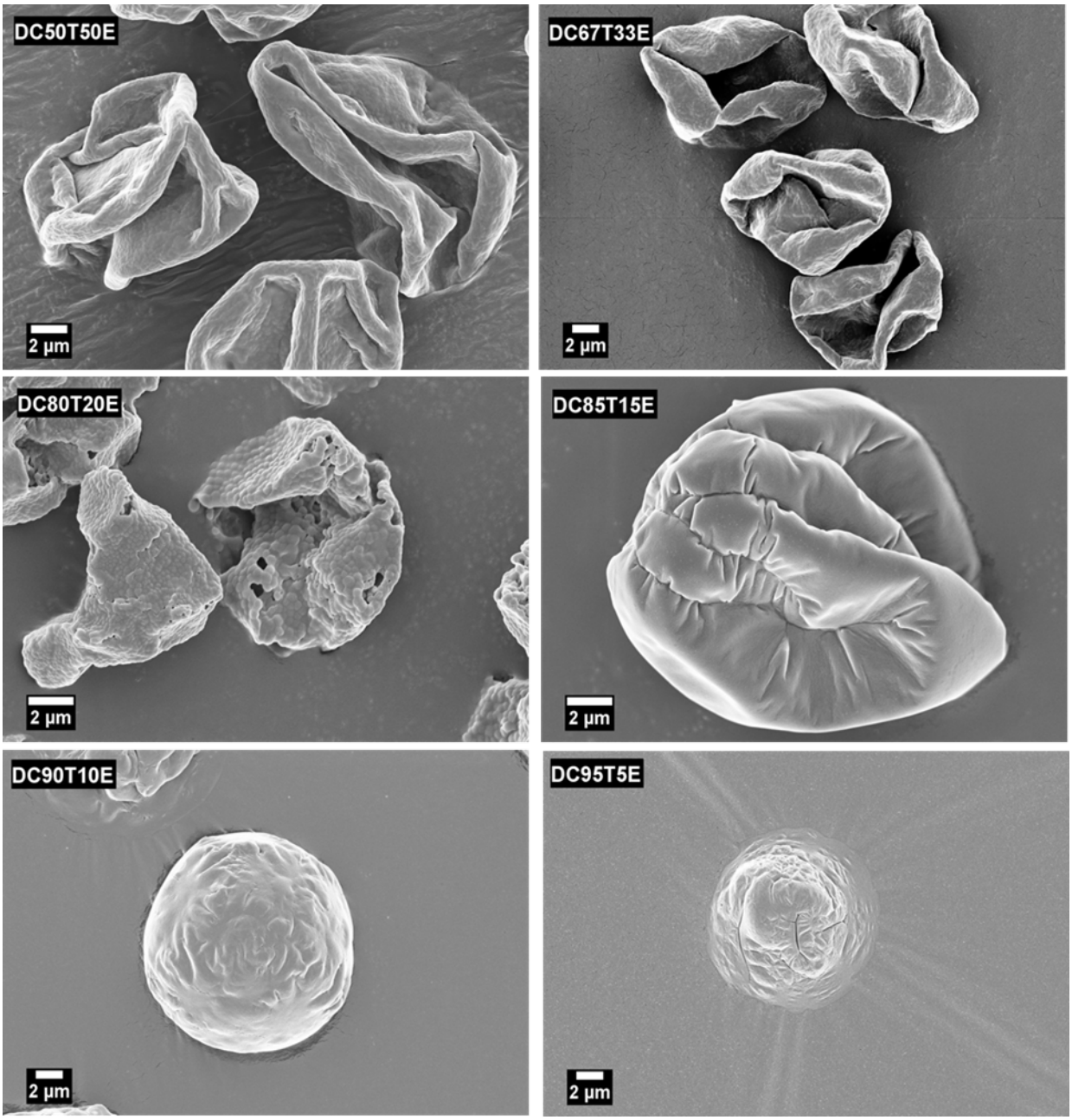

Fig. 8. SEM images of particles dried from formulations made with iso-compositional ethanol-water co-solvent, collected from the monodisperse droplet chain at 21 ˚C. Preceding numbers denote the percentage fraction of component dissolved in the solvent with respect to total solids content (10 mg/mL). The images demonstrate that particle morphology is dependent on the ratio of trehalose to Eudragit, varying from hollow and wrinkled to solid and spherical. Scale bars are shown separately for each image. Notations: DC = Droplet chain, T = trehalose, E = Eudragit.

470

3.2. Particle Formation in the Aqueous System

3.2.1. Effect of Excipient Mass Fraction on Particle Formation

For biologics that do not tolerate an organic solvent, Eudragit can also be formulated as an aqueous solution at a basic pH, which is neutralized after dissolution of the polymer. For the modeling of the particle formation process in water-based formulations, it was assumed in a first approximation that the Eudragit stays in the neutral solution in a metastable state during drying and that shell formation begins when the true density of the mixture is reached at the surface. For the low drying gas temperature of the droplet chain, the Péclet numbers of both components were lower than in the co-solvent cases, which subsequently resulted in lower surface enrichment, shown in Table 3. The effect of lower surface saturation on the radial distribution of the solids within the particles can be seen in Fig. 9. As expected, shell thickness was higher than for the iso-compositional solvent system at a higher Eudragit content, but it decreased rapidly at lower concentrations. The radial distribution profiles were comparatively flat and, for all cases except the 50:50 ratio of Eudragit and trehalose, the trehalose remained the predominant component on the surface, making the formation of a well-defined Eudragit shell under these conditions unlikely. The particle density values shown in Table 3 are consistent with particles that are fairly dense and spherical, especially at a higher trehalose content.

The morphology of the particles dried from the droplet chain did show some features that were not predicted by the model, as illustrated by the scanning electron microscopy images in Fig. 10. Particles with a higher Eudragit content showed considerable folding, thus agreeing with the trends in the model predictions. Particles composed primarily of trehalose are expected to be

spherical; however, morphological analysis showed that at lower Eudragit mass fractions the particles were more elongated and cylindrical. Moreover, the magnified images showed the presence of regularly shaped sub-domains on the surface. These are possibly sodium chloride crystals, the byproduct of a neutralization reaction to balancing the pH of the formulation. Crystallization of formulation excipients and alternative precipitation mechanisms like spinodal decomposition (Ordoubadi et al., 2021a) were not considered in the modeling of this case, so it is not surprising that the results provide only the general trends in morphological change with formulation and process conditions.

Table 3 Results of the particle formation modeling for parameters related to shell formation for different Eudragit-trehalose ratios in water-based formulations. Shown are the surface enrichment ($E_{ss,Eud}$), time to reach true density ($t_{t,mix}$) on the surface, normalized by the droplet lifetime, ($t_{t,mix}/\tau_D$); predicted particle density (ρ_P); true density of the excipient mixture ($\rho_{t,mix}$); normalized particle density ($\rho_P/\rho_{t,mix}$); and estimated shell thickness of the particles collected from the monodisperse droplet chain at 21 ˚C. Notations: DC = Droplet chain, T = trehalose, E = Eudragit.

Formulation	$\frac{t_{t,mix}}{\tau_D}$	$E_{ss,Eud}$	ρ_P (kg m^{-3})	$\rho_{t,mix}$ (kg m^{-3})	$\rho_P/\rho_{t,mix}$	**Shell Thickness (µm)**
DC50T50E(W)	0.98	1.8	710	1020	0.69	0.80
DC67T33E(W)	0.98	1.79	860	1140	0.75	0.91
DC80T20E(W)	0.98	1.77	1030	1260	0.81	0.50
DC85T15E(W)	0.98	1.75	1120	1320	0.84	0.45
DC90T10E(W)	0.98	1.70	1240	1400	0.89	0.28

DC95T5E(W)	0.99	1.67	1350	1480	0.91	0.13

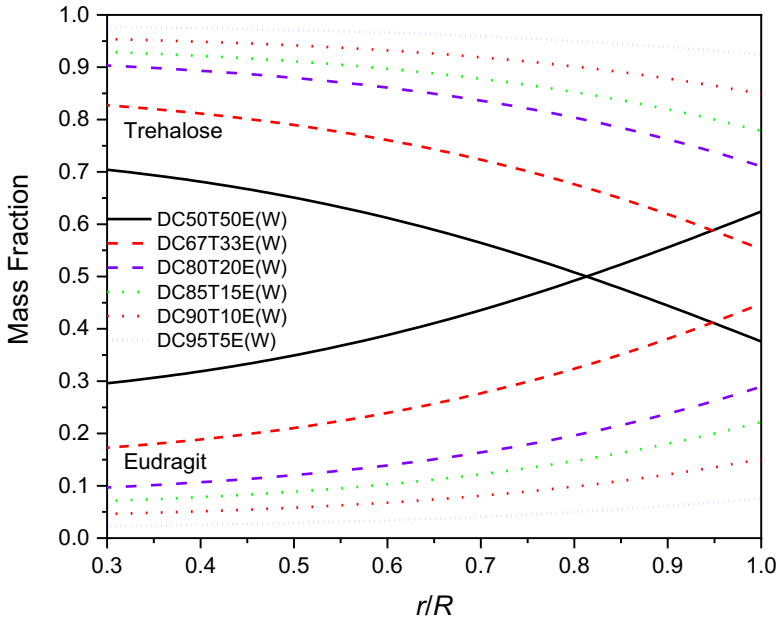

Fig.9. Radial distribution of components within the particles dried from water-based formulations at the point of predicted shell formation. Preceding numbers denote the percentage fraction of component dissolved in the solvent with respect to total solids content (10 mg/mL). A lesser amount of Eudragit reached the surface than in particles dried from ethanol-water mixtures. Notations: DC = Droplet chain, T = trehalose, E = Eudragit.

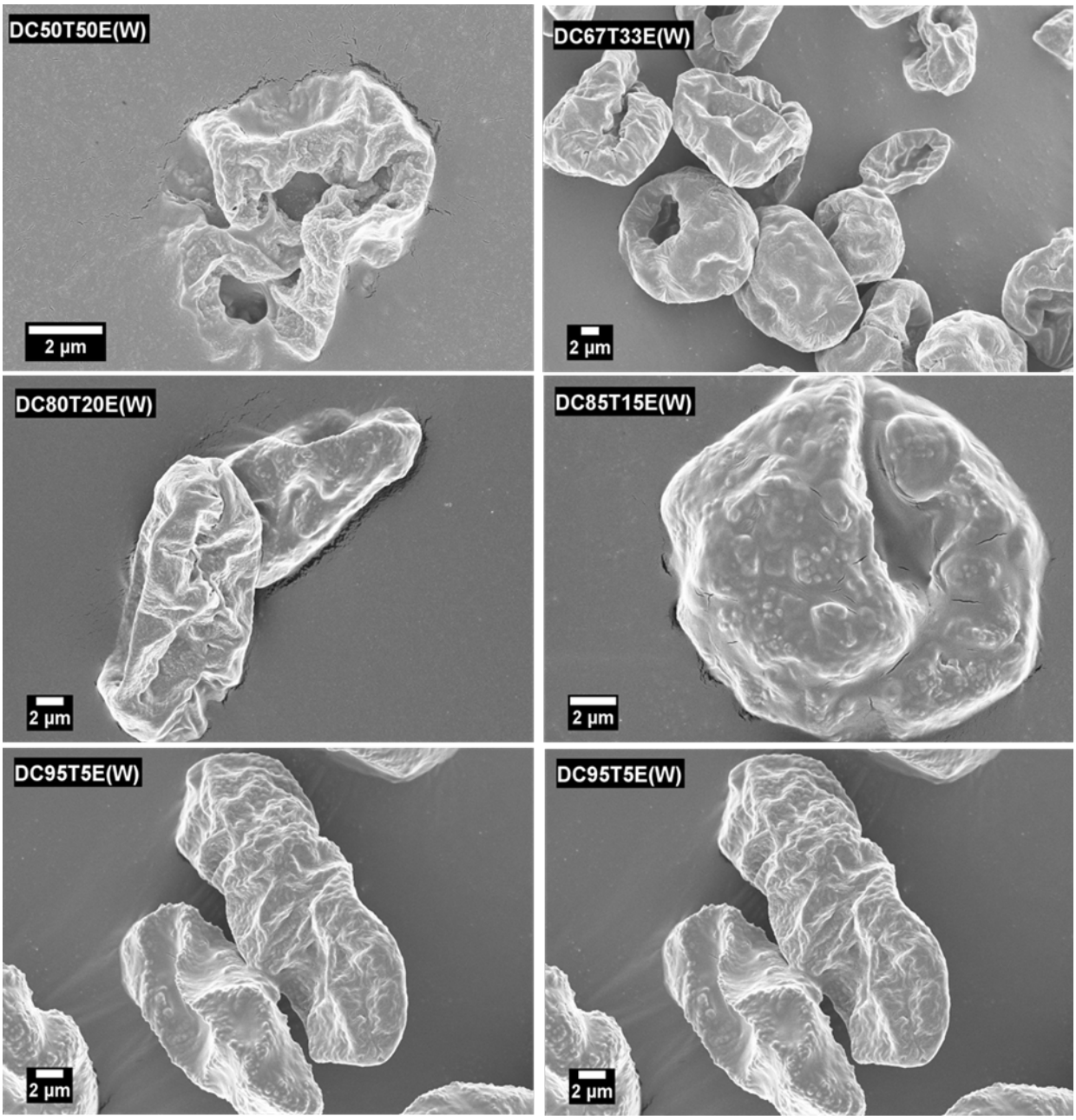

Fig. 10. SEM images showing particles dried from water-based formulations produced in a monodisperse droplet chain at 21 ˚C. The particles appeared denser with decreasing Eudragit concentrations. Scale bars are shown separately for each image.

510

3.2.2. Particle Formation at Higher Drying Temperature

To scale up the production of particles for detailed analysis, spray drying of the water-based formulations was conducted at an elevated temperature of 100 ˚C, which reduced the drying time and greatly increased the evaporation rate. As a result, the Péclet numbers and surface enrichment increased. The low density of the particles, normalized by the true density of the mixture at the time of shell formation predicts a core-shell structure and folded morphology for the spray-dried formulations. The shell thickness was calculated for the mean diameter of the dry particles, i.e., 2.2 μm. For these conditions, the shells were predicted to be less than 100 nm thick.

For diffusion-controlled particle formation, the particle morphology observed in the monodisperse droplet chain is often representative of the morphology of the spray-dried formulations (Vehring et al., 2007). In this case, the spray-dried particles showed a morphology consistent with the model predictions and are similar to the particles produced via the monodisperse droplet chain technique, as is evident from the SEM images shown in Fig. 11. Due to the higher surface enrichment, low-density particles with a folded shell were formed. Based on their surface morphology, these particles were thought likely to exhibit the targeted core-shell structure, with trehalose residing primarily towards the hollow core and Eudragit forming the shell. Previous studies have shown that trehalose can successfully be used as a stabilizer for biological components in spray-dried particles (Carrigy and Vehring, 2019). However, it was necessary to determine the limiting concentration of Eudragit capable of providing proper protection to the encapsulated active component. Hence, the spray-dried batches were selected for the dissolution test.

Table 4 Results of the particle formation modeling for parameters related to shell formation for different Eudragit-trehalose ratios in water-based formulations. Shown are the surface enrichment ($E_{ss,Eud}$), predicted particle density (ρ_P), true density of the excipient mixture ($\rho_{t,mix}$), normalized particle density ($\rho_P/\rho_{t,mix}$), and estimated shell thickness of the particles spray-dried at 100 ˚C. Notations: SD = spray-dried, T = trehalose, E = Eudragit.

Formulation	$\boldsymbol{E_{ss,Eud}}$	$\boldsymbol{\rho_P}$ **(kg m^{-3})**	$\boldsymbol{\rho_{t,mix}}$ **(kg m^{-3})**	$\boldsymbol{\rho_P/\rho_{t,mix}}$	**Shell Thickness (nm)**
SD80T20E	3.58	315	1160	0.27	94
SD85T15E	3.58	310	1220	0.25	88
SD90T10E	3.58	310	1300	0.24	84
SD95T5E	3.57	310	1420	0.22	81
SD97T3E	3.57	310	1470	0.21	80
SD99T1E	3.57	310	1540	0.20	78

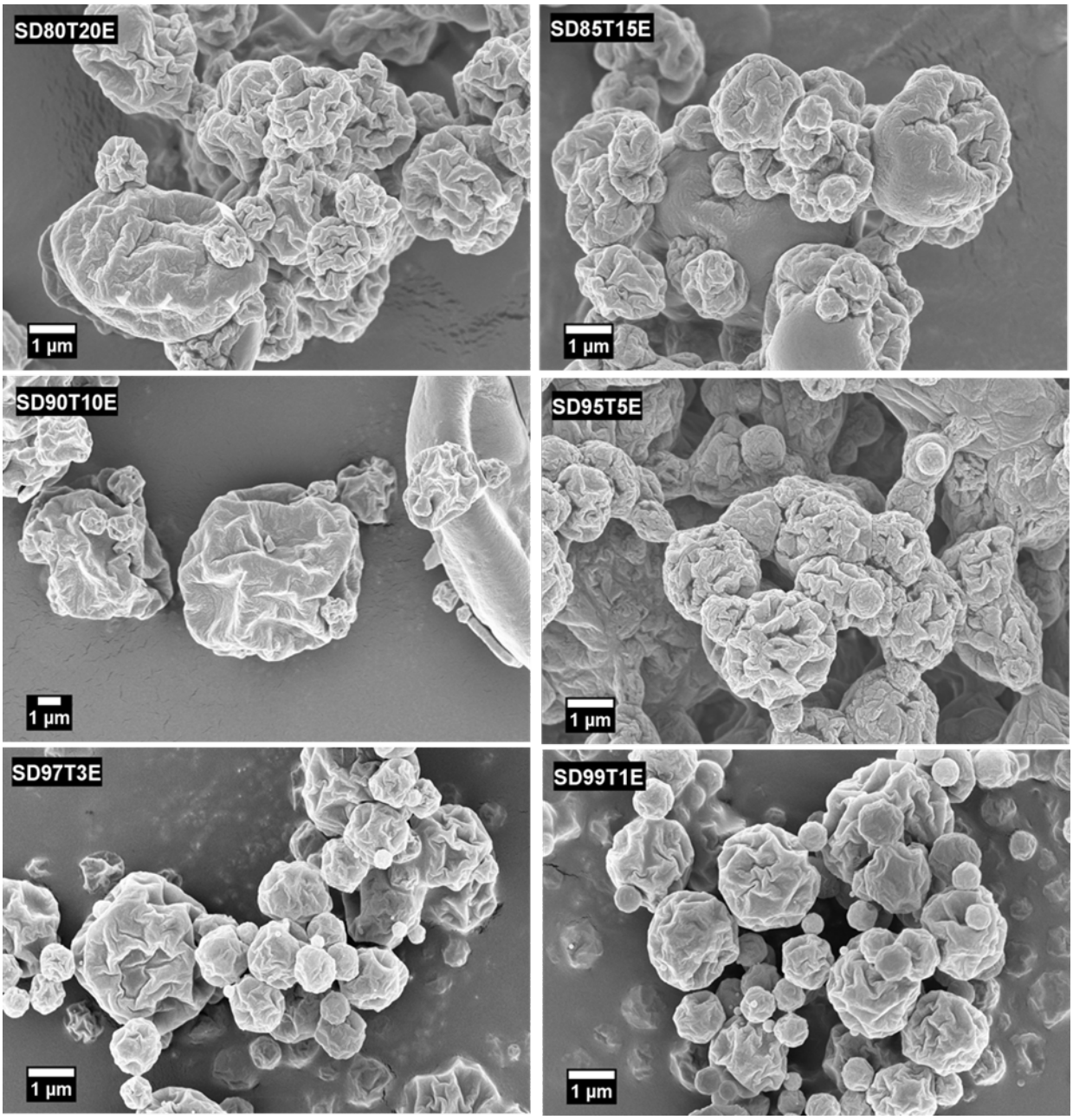

Fig. 11. SEM images showing the morphology of the spray-dried particles at 100 ˚C. Preceding numbers denote the percentage fractions of components dissolved in the solvent with respect to total solids content (20 mg/mL). Scale bars are shown separately for each image. Notations: SD = spray-dried, T = trehalose, E = Eudragit.

3.3. Particle Dissolution in Acidic and Alkaline Media

The purpose of conducting the dissolution test was to observe the duration and degree of survival of the particles in simulated gastric conditions. The typical pH of the human stomach ranges from 1.8 to 2.8 (Ovesen et al., 1986), whereas the pH in the intestine can range from 6 to 8 depending on specific regions (small intestine, large intestine, colon) (Evans et al., 1988; Ibekwe et al., 2008). The mean gastric emptying time in humans is 1.1 hours, but this can vary depending on different factors (Lysgård Madsen, 1992). The particles must be able to withstand the corrosive environment of the gastrointestinal tract for an extended period of time in order to successfully deliver a therapeutic to the enteric system.

The dissolution of the spray-dried aqueous formulations suspended in an HCL-water solution (pH = 2) was expressed in terms of the transmission coefficient, as shown in Fig. 12. The coefficient ranges from 0 to 1, with 0 indicating no change in light intensity passing through the suspension during the test and 1 indicating total clarification of the suspension, which was interpreted as complete dissolution of the particles in the medium. As a control, Eudragit raw material was first suspended in the medium. The suspension remained unchanged after one hour of mechanical stirring, which was reflected in the relatively constant transmission coefficient. This result was expected because of Eudragit S100's insolubility at low pH values. The spray-dried powders, which were polydisperse with varying morphology and particle sizes, showed different levels of change in the transmission coefficient, depending on the Eudragit content. Particles with the largest Eudragit contents of 10 to 20% maintained a small transmission coefficient over time, indicating that most of the polydisperse particles did not dissolve. By contrast, the formulations containing 1 and 3% Eudragit showed a very sharp rise in the transmission coefficient, consistent

with the almost immediate dissolution observed during the test. The case involving 5 % Eudragit showed intermediate behavior with ongoing dissolution over time.

As the Eudragit fraction in the formulations is reduced, the concentration of Eudragit at the surface decreases relative to that of trehalose. For the formulations with low Eudragit content this makes the shell susceptible to corrosion by hydrochloric acid. However, formulations SD80T20E, SD85T15E and SD90T10E showed promising results for protection against stomach acid, as the change in transmission coefficient was very small over one hour, indicating a relatively small change in suspension concentration in the medium due to corrosion or dissolution.

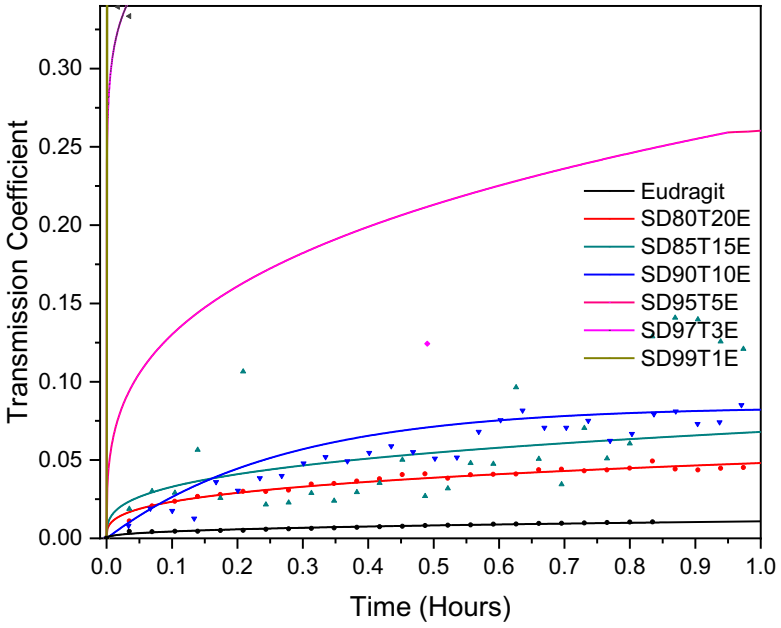

Fig.12. Dissolution behavior as approximated by the optical transmission coefficient for suspensions of different spray-dried powders in an acidic medium (pH 2). Samples with high Eudragit content (SD80T20E, SD85T15E, SD90T10E) showed a very small change in coefficient

over time, while SD95T5E dissolved significantly over time, which is reflected in an intermediate value of transmission coefficient. SD97T3E; SD99T1E dissolved almost instantly.

Fig. 13 shows the dissolution profiles in an alkaline medium simulating the desired dissolution of the particles in the intestines. During two hours of mechanical stirring, the transmission coefficient increased gradually for all the suspensions. Similarly, formulations with more Eudragit
575 demonstrated a slower dissolution rate. The changes in the transmission coefficients were larger and faster than the results for the acidic medium, indicating a more rapid dissolution of particles in the alkaline medium. These results indicate that Eudragit layers on spray-dried particles can be designed to provide a specific release profile, making this approach promising for enteric delivery.

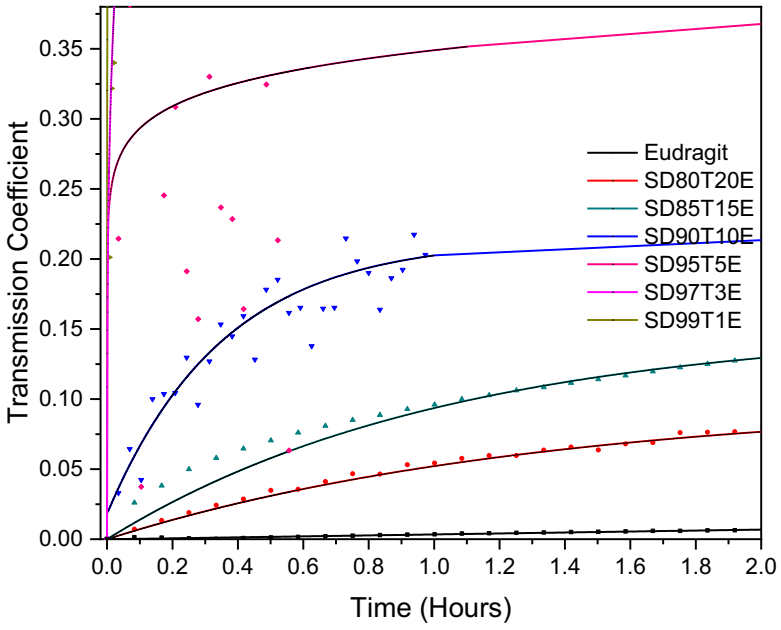

Fig. 13. Dissolution behavior as approximated by the optical transmission coefficient for suspensions of different spray-dried powders in an alkaline medium (pH 8). Samples SD80T20E,

SD85T15E and SD90T10E showed a gradual increase in transmission intensity over time for two hours, indicating their delayed release pattern. SD95T5E had a relatively higher transmission coefficient, whereas SD97T3E and SD99T1E dissolved in the medium instantly.

3.4. Analysis of Particles Subjected to Suspension in Acid

The Raman spectra of the filtered and dried suspensions were analyzed to determine the solid phase of trehalose in the residual powder that remained after the dissolution test in the acidic medium. A failure of the protective shell is expected to lead to water ingress into the trehalose core, which can in turn lead to trehalose crystallization or even dissolution. It is important to know if the core is exposed to moisture because a change in the solid phase of trehalose from amorphous to crystalline can inactivate biologics such as bacteriophages (Vandenheuvel et al., 2014). Fig. 14 shows the reference spectra for amorphous and crystalline trehalose, and amorphous Eudragit that were used to deconvolute the measured spectra of the four dried suspensions that did not dissolve. The suspension spectra and their deconvoluted residual spectra are shown in Fig. 15.

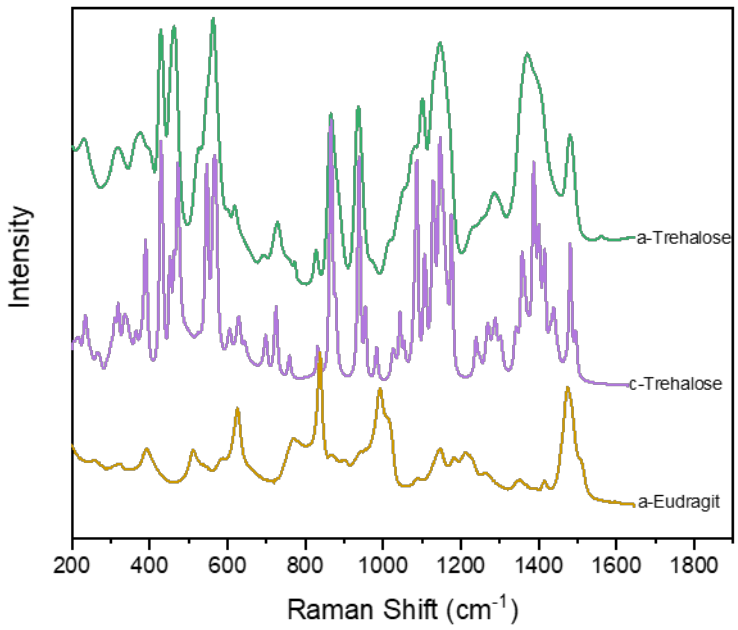

Fig. 14. Reference spectra of amorphous and crystalline trehalose and amorphous Eudragit used for deconvolution.

The deconvolution of the Raman spectrum of the recovered suspension SD80T20E showed the trehalose present to be fully amorphous. The 10 and 15% Eudragit-containing formulations had only a small amount of crystalline trehalose. However, the trehalose in the 5% Eudragit formulation had predominantly converted into the crystalline form. The presence of both trehalose and Eudragit in a ratio close to the initial formulation composition in SD80T20E proved that the trehalose core of the particles stayed largely intact even after one hour of exposure to acidic conditions. The intensity ratios of crystalline and amorphous trehalose and amorphous Eudragit within the dried suspensions were calculated using a custom-designed dispersive Raman spectroscopy and deconvolution method described elsewhere (Wang et al., 2017a). The results are shown in Table 5. All measurements were triplicated, with the relative standard deviations

representing the source of uncertainty in the calculations. The measured intensity ratios represent the presence of different components in the formulations and are proportional to the mass fraction ratios of the components, which can be related using calibration factors.

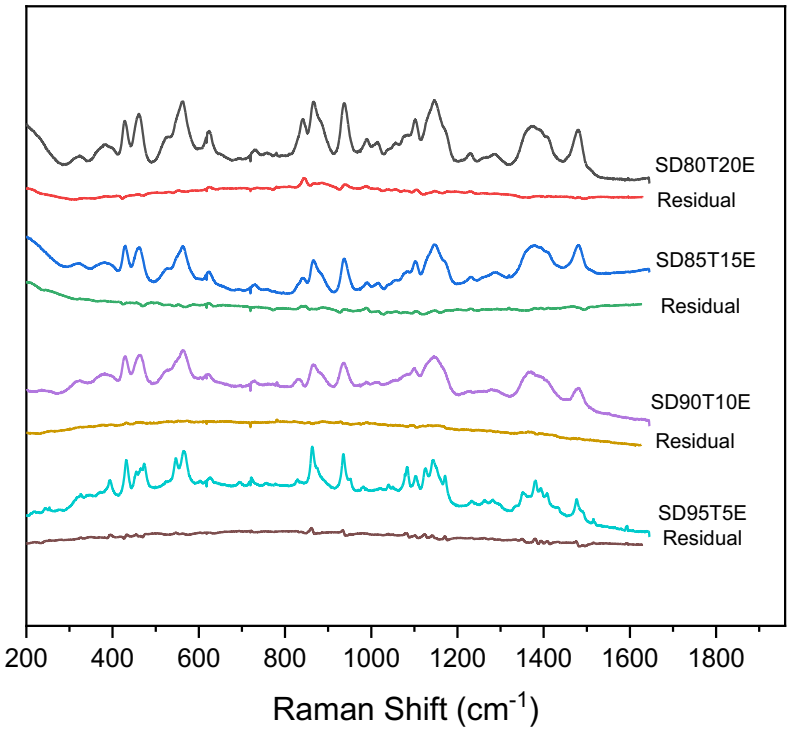

Fig. 15. Residual spectra of the cured samples are shown underneath their Raman spectra. A primarily amorphous structure is seen in all samples. Deconvolution of SD85T15E and SD90T10E showed trace amounts of crystalline trehalose, whereas SD95T5E showed the presence of a high amount of crystalline trehalose.

A coating with a thickness on the order of 100 nm (cf. Table 4) in formulation SD80T20E withstood the low pH well enough to keep the core sufficiently protected from water ingress, a result that was confirmed by the absence of crystalline trehalose in the dried suspension. Exposure to the surrounding medium would either dissolve or crystallize the trehalose, neither of which events

occurred. The intensity factor ratio of crystalline trehalose increased with a decrease in the amount of Eudragit in the formulations, a result that points to an increased presence of the crystalline component in the dried suspensions. In the case of formulation SD95T5E, the intensity factor ratio of amorphous trehalose decreased dramatically, indicating partial dissolution, whereas the increase in intensity factor ratio of crystalline trehalose was high, indicating that much of the remaining trehalose was crystalline. This result confirmed that at low Eudragit content the particle core could not be protected from water ingress after exposure to low pH, making the particles unsuitable for an enteric application. The results also suggest that a rather small mass fraction of Eudragit in the formulations (20%), and consequently a relatively thin shell, may be sufficient to ensure protection against an acidic environment.

Table 5 Data showing the intensity factor ratio of amorphous trehalose-amorphous Eudragit ($\frac{I_{a-tre}}{I_{Eud}}$) and crystalline trehalose-amorphous Eudragit ($\frac{I_{c-tre}}{I_{Eud}}$) obtained from deconvolution of the Raman spectra of powder recovered from the acidic medium after one hour of exposure. The relative standard deviation (RSD) represents the error in calculation.

Sample	$\frac{I_{\mathrm{a-tre}}}{I_{\mathrm{Eud}}}$	**RSD (%)**	$\frac{I_{\mathrm{c-tre}}}{I_{\mathrm{Eud}}}$	**RSD (%)**
SD80T20E	1.33	1.2	0	-
SD85T15E	1.67	0.5	0.10	29
SD90T10E	2.33	0.7	0.23	8
SD95T5E	1.33	1.7	0.83	6

4. Conclusion

This study describes the application of particle engineering principles in developing microparticles capable of encapsulating active pharmaceutical ingredients with a pH-responsive polymer via spray drying. The particle formation process of an Eudragit-trehalose system was evaluated at different cosolvent ratios of ethanol-water and in water. The effectiveness of the spray-dried particles against potentially harsh conditions of the gastrointestinal tract was tested by suspending spray-dried particles in solutions simulating gastric conditions and tracking the light transmission intensity through the suspension samples using a new shadowgraphic imaging technique. The results of the preliminary studies showed that irrespective of the type of solvent used, it is possible to design particles with a trehalose core and a Eudragit shell of varying thickness. The results further showed that, as an alternative to subjecting biologics to the stresses of a multi-step tableting process, spray drying can likely simplify the coating process into a single step. The product in powdered form has the potential to provide protection for therapeutics, particularly biologic components, and can be administered as a suspension, simplifying administration to pediatric and geriatric populations that struggle with swallowing tablets. With appropriate understanding, it appears feasible to design and produce microparticles that can protect biologics such as bacteriophages against harsh gastrointestinal conditions, and the potential demonstrated by the spray-dried powders makes them promising candidates for delivery of biologics to human or animal enteric systems via the oral route.

Because of the limitations of the lab-scale spray dryer used in this study, the particle size of the studied powders was limited to less than 5 µm, smaller than what would be appropriate for oral

delivery. Pilot-scale spray driers, however, are capable of producing particles in the range of 50 µm or larger. Spray drying large particles containing phages and conducting *in vitro* stability studies of the product at elevated temperatures and humidities would be the next logical steps for this research.

References

Abdelsattar, A.S., Abdelrahman, F., Dawoud, A., Connerton, I.F., El-Shibiny, A., 2019. Encapsulation of E. coli phage ZCEC5 in chitosan–alginate beads as a delivery system in phage therapy. AMB Express 9. https://doi.org/10.1186/s13568-019-0810-9

Al-Zoubi, N., AlKhatib, H.S., Bustanji, Y., Aiedeh, K., Malamataris, S., 2008. Sustained-release of buspirone HCl by co spray-drying with aqueous polymeric dispersions. Eur. J. Pharm. Biopharm. 69, 735–742. https://doi.org/10.1016/j.ejpb.2008.01.002

Amiet-Charpentier, C., Gadille, P., Digat, B., Benoit, J.P., 1998. Microencapsulation of rhizobacteria by spray-drying: Formulation and survival studies. J. Microencapsul. 15, 639–659. https://doi.org/10.3109/02652049809008247

Año, G., Esquisabel, A., Pastor, M., Talavera, A., Cedré, B., Fernández, S., Sifontes, S., Aranguren, Y., Falero, G., García, L., Solís, R.L., Pedraz, J.L., 2011. A new oral vaccine candidate based on the microencapsulation by spray-drying of inactivated Vibrio cholerae. Vaccine 29, 5758–5764. https://doi.org/10.1016/j.vaccine.2011.05.098

Ashkenazi, S., Levy, I., Kazaronovski, V., Samra, Z., 2003. Growing antimicrobial resistance of Shigella isolates. J. Antimicrob. Chemother. 51, 427–429. https://doi.org/10.1093/jac/dkg080

Bora, D., Borude, P., Bhise, K., 2008. Taste masking by spray-drying technique. AAPS PharmSciTech 9, 1159–1164. https://doi.org/10.1208/s12249-008-9154-5

Boraey, M.A., Vehring, R., 2014. Diffusion controlled formation of microparticles. J. Aerosol Sci.

67, 131–143. https://doi.org/10.1016/j.jaerosci.2013.10.002

Carrigy, N.., Vehring, R., 2019. Engineering stable spray-dried biologic powder for inhalation, in: Anthony J. Hickey, Sandro R.P. da Rocha (Eds.), Pharmacuetical Inhalation Aerosol Technology. CRC Press, Boca Raton, pp. 291–326. https://doi.org/https://doi.org/10.1201/9780429055201

Carrigy, N.B., Liang, L., Wang, H., Kariuki, S., Nagel, T.E., Connerton, I.F., Vehring, R., 2020. Trileucine and Pullulan Improve Anti-Campylobacter Bacteriophage Stability in Engineered Spray-Dried Microparticles. Ann. Biomed. Eng. 48, 1169–1180. https://doi.org/10.1007/s10439-019-02435-6

Carrigy, N.B., Ordoubadi, M., Liu, Y., Melhem, O., Barona, D., Wang, H., Milburn, L., Ruzycki, C.A., Finlay, W.H., Vehring, R., 2019. Amorphous pullulan trehalose microparticle platform for respiratory delivery. Int. J. Pharm. 563, 156–168. https://doi.org/10.1016/j.ijpharm.2019.04.004

Cerea, M., Zheng, W., Young, C.R., McGinity, J.W., 2004. A novel powder coating process for attaining taste masking and moisture protective films applied to tablets. Int. J. Pharm. 279, 127–139. https://doi.org/10.1016/j.ijpharm.2004.04.015

Chiu, C.-H., Wu, T.-L., Su, L.-H., Chu, C., Chia, J.-H., Kuo, A.-J., Chien, M.-S., Lin, T.-Y., 2002. The Emergence In Taiwan Of Fluroquinolone Resistance In Salmonella Enterica Serotype Choleraesuis. N. Engl. J. Med. 346. https://doi.org/10.1056/NEJMoa012261.

Das, S., Suresh, P.K., Desmukh, R., 2010. Design of Eudragit RL 100 nanoparticles by nanoprecipitation method for ocular drug delivery. Nanomedicine Nanotechnology, Biol. Med. 6, 318–323. https://doi.org/10.1016/j.nano.2009.09.002

De Smet, R., Verschuere, S., Allais, L., Leclercq, G., Dierendonck, M., De Geest, B.G., Van Driessche, I., Demoor, T., Cuvelier, C.A., 2014. Spray-dried polyelectrolyte microparticles in oral antigen delivery: Stability, biocompatibility, and cellular uptake. Biomacromolecules 15, 2301–2309. https://doi.org/10.1021/bm5005367

Drašković, M., Medarević, D., Aleksić, I., Parojčić, J., 2017. In vitro and in vivo investigation of taste-masking effectiveness of Eudragit E PO as drug particle coating agent in orally disintegrating tablets. Drug Dev. Ind. Pharm. 43, 723–731. https://doi.org/10.1080/03639045.2016.1220572

Edward, J.T., 1970. Molecular Volumes and the Stokes-Einstein Equation. J. Chem. Educ. 47, 261–270. https://doi.org/https://doi.org/10.1021/ed047p261

El-Malah, Y., Nazzal, S., 2008. Novel use of Eudragit® NE 30D/Eudragit® L 30D-55 blends as functional coating materials in time-delayed drug release applications. Int. J. Pharm. 357, 219–227. https://doi.org/10.1016/j.ijpharm.2008.02.003

Evans, D.F., Pye, G., Bramley, R., Clark, A.G., Dyson, T.J., Hardcastle, J.D., 1988. Measurement of gastrointestinal pH profiles in normal ambulant human subjects. Gut 29, 1035–1041. https://doi.org/10.1136/gut.29.8.1035

Evonik Industries, 2012. Technical Information EUDRAGIT® L 100 and EUDRAGIT® S 100. Evonik Ind. AG. URL http://eudragit.evonik.com/sites/lists/HN/ProductSpecifications/TI-EUDRAGIT-L-100-S-100-EN.pdf (accessed 2.23.21).

Glass, R.I., Huq, I., Alim a., A.R.M., Yunus, M., 1980. Emergence of multiply antibiotic-resistant Vibrio cholerae in Bangladesh. J. Infect. Dis. 142, 939–942. https://doi.org/10.1093/infdis/142.6.939

Grasmeijer, N., Frijlink, H.W., Hinrichs, W.L.J., 2016. Model to predict inhomogeneous protein–sugar distribution in powders prepared by spray drying. J. Aerosol Sci. 101, 22–33. https://doi.org/10.1016/j.jaerosci.2016.07.012

Hesselbacher, K.H., Anders, K., Frohn, A., 1991. Experimental investigation of Gaussian beam effects on the accuracy of a droplet sizing method. Appl. Opt. 30, 4930. https://doi.org/10.1364/ao.30.004930

Hoe, S., Ivey, J.W., Boraey, M.A., Shamsaddini-Shahrbabak, A., Javaheri, E., Matinkhoo, S., Finlay, W.H., Vehring, R., 2014. Use of a fundamental approach to spray-drying formulation design

to facilitate the development of multi-component dry powder aerosols for respiratory drug delivery. Pharm. Res. 31, 449–465. https://doi.org/10.1007/s11095-013-1174-5

Ibekwe, V.C., Fadda, H.M., McConnell, E.L., Khela, M.K., Evans, D.F., Basit, A.W., 2008. Interplay between intestinal pH, transit time and feed status on the in vivo performance of pH responsive ileo-colonic release systems. Pharm. Res. 25, 1828–1835. https://doi.org/10.1007/s11095-008-9580-9

Ivey, J., Bhambri, P., Lewis, D., Church, T., Finlay, W., Vehring, R., 2016. Dried corticosteroid particle formation from evaporating monodisperse propellant solution droplets, in: AAPS Annual Meeting and Exposition. Denver.

Ivey, J.W., Vehring, R., 2010. The use of modeling in spray drying of emulsions and suspensions accelerates formulations and process development. Comput. Chem. Eng. 34, 1036–1040. https://doi.org/https://doi.org/10.1016/j.compchemeng.2010.02.031

Jończyk, E., Kłak, M., Międzybrodzki, R., Górski, A., 2011. The influence of external factors on bacteriophages-review. Folia Microbiol. (Praha). 56, 191–200. https://doi.org/10.1007/s12223-011-0039-8

Kim, Y.D., Morr, C. V., Schenz, T.W., 1996. Microencapsulation Properties of Gum Arabic and Several Food Proteins: Liquid Orange Oil Emulsion Particles. J. Agric. Food Chem. 44, 1308–1313. https://doi.org/10.1021/jf950391e

Koo, J., DePaola, A., Marshall, D.L., 2000. Effect of simulated gastric fluid and bile on survival of Vibrio vulnificus and Vibrio vulnificus phage†. J. Food Prot. 63, 1665–1669. https://doi.org/10.4315/0362-028X-63.12.1665

Koo, J., Marshall, D.L., DePaola, A., 2001. Antacid Increases Survival of Vibrio vulnificus and Vibrio vulnificus Phage in a Gastrointestinal Model. Appl. Environ. Microbiol. 67, 2895–2902. https://doi.org/10.1128/AEM.67.7.2895-2902.2001

Kristmundsdóttir, T., Gudmundsson, Ó.S., Ingvarsdóttir, K., 1996. Release of diltiazem from Eudragit microparticles prepared by spray-drying. Int. J. Pharm. 137, 159–165.

https://doi.org/10.1016/0378-5173(96)04509-7

Kunda, N.K., Alfagih, I.M., Miyaji, E.N., Figueiredo, D.B., Gonçalves, V.M., Ferreira, D.M., Dennison, S.R., Somavarapu, S., Hutcheon, G.A., Saleem, I.Y., 2015. Pulmonary dry powder vaccine of pneumococcal antigen loaded nanoparticles. Int. J. Pharm. 495, 903–912. https://doi.org/10.1016/j.ijpharm.2015.09.034

Leung, S.S.Y., Parumasivam, T., Nguyen, A., Gengenbach, T., Carter, E.A., Carrigy, N.B., Wang, H., Vehring, R., Finlay, W.H., Morales, S., Britton, W.J., Kutter, E., Chan, H.K., 2018. Effect of storage temperature on the stability of spray dried bacteriophage powders. Eur. J. Pharm. Biopharm. 127, 213–222. https://doi.org/10.1016/j.ejpb.2018.02.033

Lunter, D.J., Daniels, R., 2012. New film forming emulsions containing Eudragit® NE and/or RS 30D for sustained dermal delivery of nonivamide. Eur. J. Pharm. Biopharm. 82, 291–298. https://doi.org/10.1016/j.ejpb.2012.06.010

Lysgård Madsen, J., 1992. Effects of gender, age, and body mass index on gastrointestinal transit times. Dig. Dis. Sci. 37, 1548–1553. https://doi.org/10.1007/BF01296501

Matinkhoo, S., Lynch, K.H., Dennis, J.J., Finlay, W.H., Vehring, R., 2011. Spray-Dried Respirable Powders Containing Bacteriophages for the Treatment of Pulmonary Infections. J. Pharm. Sci. 100, 5197–5205. https://doi.org/https://doi.org/10.1002/jps.22715

Mwansa, J.C.L., Mwaba, J., Lukwesa, C., Bhuiyan, N.A., Ansaruzzaman, M., Ramamurthy, T., Alam, M., Balakrish, G., 2007. Multiply antibiotic-resistant Vibrio cholerae O1 biotype El Tor strains emerge during cholera outbreaks in Zambia. Epidemiol. Infect. 135, 847–853. https://doi.org/10.1017/S0950268806007254

Ordoubadi, M., Gregson, F.K.A., Melhem, O., Barona, D., Miles, R.E.H., D'Sa, D., Gracin, S., Lechuga-Ballesteros, D., Reid, J.P., Finlay, W.H., Vehring, R., 2019. Multi-Solvent Microdroplet Evaporation: Modeling and Measurement of Spray-Drying Kinetics with Inhalable Pharmaceutics. Pharm. Res. 36. https://doi.org/10.1007/s11095-019-2630-7

Ordoubadi, M., Gregson, F.K.A., Wang, H., Carrigy, N.B., Nicholas, M., Gracin, S., Lechuga-,

Lechuga-Ballesteros, D., Reid, J.P., Finlay, W.H., Vehring, R., 2021a. Trileucine as a dispersibility enhancer of spray-dried inhalable microparticles. J. Control. Release. https://doi.org/https://doi.org/10.1016/j.jconrel.2021.06.045

Ordoubadi, M., Gregson, F.K.A., Wang, H., Nicholas, M., Gracin, S., Lechuga-Ballesteros, D., Reid, J.P., Finlay, W.H., Vehring, R., 2021b. On the particle formation of leucine in spray drying of inhalable microparticles. Int. J. Pharm. 592, 120102. https://doi.org/10.1016/j.ijpharm.2020.120102

Ovesen, L., Bendtsen, F., Tage-Jensen, U., Pedersen, N.T., Gram, B.R., Rune, S.J., 1986. Intraluminal pH in the stomach, duodenum, and proximal jejunum in normal subjects and patients with exocrine pancreatic insufficiency. Gastroenterology 90, 958–962. https://doi.org/10.1016/0016-5085(86)90873-5

Perumal, D., 2001. Microencapsulation of ibuprofen and Eudragit RS 100 by the emulsion solvent evaporation technique 218, 1–11. https://doi.org/10.1016/s0378-5173(00)00686-4

Pradhan, R., Kim, S.Y., Yong, C.S., Kim, J.O., 2016. Preparation and characterization of spray-dried valsartan-loaded Eudragit® E PO solid dispersion microparticles. Asian J. Pharm. Sci. 11, 744–750. https://doi.org/10.1016/j.ajps.2016.05.002

Rassu, G., Gavini, E., Spada, G., Giunchedi, P., Marceddu, S., 2008. Ketoprofen spray-dried microspheres based on eudragit® RS and RL: Study of the manufacturing parameters. Drug Dev. Ind. Pharm. 34, 1178–1187. https://doi.org/10.1080/03639040801974303

Reinthaler, F.F., Posch, J., Feierl, G., Wüst, G., Haas, D., Ruckenbauer, G., Mascher, F., Marth, E., 2003. Antibiotic resistance of E. Coli in sewage and sludge. Water Res. 37, 1685–1690. https://doi.org/10.1016/S0043-1354(02)00569-9

Rowe, R.C., Sheskey, P.J., Quinn, M.E., 2009. Handbook of pharmaceutical excipients, 7th ed, Libros Digitales-Pharmaceutical Press. https://doi.org/https://doi.org/10.3109/10837450.2012.751408

Saboo, S., Tumban, E., Peabody, J., Wafula, D., Peabody, D.S., Chackerian, B., Muttil, P., 2016.

Optimized Formulation of a Thermostable Spray-Dried Virus-Like Particle Vaccine against Human Papillomavirus. Mol. Pharm. 13, 1646–1655. https://doi.org/10.1021/acs.molpharmaceut.6b00072

Sauer, D., Cerea, M., Dinunzio, J., McGinity, J., 2013. Dry powder coating of pharmaceuticals: A review. Int. J. Pharm. 457, 488–502. https://doi.org/10.1016/j.ijpharm.2013.02.032

Schuck, P., 2002. Spray drying of dairy products: state of the art. Lait 82, 375–382. https://doi.org/10.1051/lait

Serrano, D.R., Persoons, T., D'Arcy, D.M., Galiana, C., Dea-Ayuela, M.A., Healy, A.M., 2016. Modelling and shadowgraph imaging of cocrystal dissolution and assessment of in vitro antimicrobial activity for sulfadimidine/4-aminosalicylic acid cocrystals. Eur. J. Pharm. Sci. 89, 125–136. https://doi.org/10.1016/j.ejps.2016.04.030

Sóti, P.L., Bocz, K., Pataki, H., Eke, Z., Farkas, A., Verreck, G., Kiss, É., Fekete, P., Vigh, T., Wagner, I., Nagy, Z.K., Marosi, G., 2015. Comparison of spray drying, electroblowing and electrospinning for preparation of Eudragit E and itraconazole solid dispersions. Int. J. Pharm. 494, 23–30. https://doi.org/10.1016/j.ijpharm.2015.07.076

Sou, T., Morton, D.A.V., Williamson, M., Meeusen, E.N., Kaminskas, L.M., McIntosh, M.P., 2015. Spray-Dried Influenza Antigen with Trehalose and Leucine Produces an Aerosolizable Powder Vaccine Formulation that Induces Strong Systemic and Mucosal Immunity after Pulmonary Administration. J. Aerosol Med. Pulm. Drug Deliv. 28, 361–371. https://doi.org/10.1089/jamp.2014.1176

Thakral, S., Thakral, N.K., Majumdar, D.K., 2013. Eudragit®: A technology evaluation. Expert Opin. Drug Deliv. 10, 131–149. https://doi.org/10.1517/17425247.2013.736962

Trung, V.N., Phung, V. Le, Chinh, H. Le, Weintraub, A., 2005. Antibiotic resistance in diarrheagenic Escherichia coli and Shigella strains isolated from children in Hanoi, Vietnam. Antimicrob. Agents Chemother. 49, 816–819. https://doi.org/10.1128/AAC.49.2.816-819.2005

van den Bogaard, A.E., London, N., Driessen, C., Stobberingh, E.E., 2001. Antibiotic resistance of

825 faecal Escherichia coli in poultry, poultry farmers and poultry slaughterers. J. Antimicrob. Chemother. 47, 763–771. https://doi.org/10.1093/jac/47.6.763

Vandenheuvel, D., Meeus, J., Lavigne, R., Van Den Mooter, G., 2014. Instability of bacteriophages in spray-dried trehalose powders is caused by crystallization of the matrix. Int. J. Pharm. 472, 202–205. https://doi.org/10.1016/j.ijpharm.2014.06.026

830 Vehring, R., 2008. Pharmaceutical particle engineering via spray drying. Pharm. Res. 25, 999–1022. https://doi.org/10.1007/s11095-007-9475-1

Vehring, R., 2005. Red-excitation dispersive Raman spectroscopy is a suitable technique for solid-state analysis of respirable pharmaceutical powders. Appl. Spectrosc. 59, 286–292. https://doi.org/10.1366/0003702053585318

835 Vehring, R., Foss, W.R., Lechuga-Ballesteros, D., 2007. Particle formation in spray drying. J. Aerosol Sci. 38, 728–746. https://doi.org/10.1016/j.jaerosci.2007.04.005

Vinner, G.K., Rezaie-Yazdi, Z., Leppanen, M., Stapley, A.G.F., Leaper, M.C., Malik, D.J., 2019. Microencapsulation of Salmonella-specific bacteriophage felix o1 using spray-drying in a ph-responsive formulation and direct compression tableting of powders into a solid oral dosage 840 form. Pharmaceuticals 12, 1–14. https://doi.org/10.3390/ph12010043

Wang, H., Barona, D., Oladepo, S., Williams, L., Hoe, S., Lechuga-Ballesteros, D., Vehring, R., 2017a. Macro-Raman spectroscopy for bulk composition and homogeneity analysis of multi-component pharmaceutical powders. J. Pharm. Biomed. Anal. 141, 180–191. https://doi.org/10.1016/j.jpba.2017.04.003

845 Wang, H., Bhambri, P., Ivey, J., Vehring, R., 2017b. Design and pharmaceutical applications of a low-flow-rate single-nozzle impactor. Int. J. Pharm. 533, 14–25. https://doi.org/10.1016/j.ijpharm.2017.09.047

Wang, H., Tan, P., Barona, D., Li, G., Hoe, S., Lechuga-Ballesteros, D., Nobes, D.S., Vehring, R., 2018. Characterization of the suspension stability of pharmaceuticals using a shadowgraphic 850 imaging method. Int. J. Pharm. 548, 128–138.

https://doi.org/10.1016/j.ijpharm.2018.06.053

World Health Organization, 2014. Antimicrobial resistance: global report on surveillance.

Yoke-Kqueen, C., Learn-Han, L., Noorzaleha, A.S., Son, R., Sabrina, S., Jiun-Horng, S., Chai-Hoon, K., 2008. Characterization of multiple-antimicrobial-resistant Salmonella enterica Subsp. enterica isolated from indigenous vegetables and poultry in Malaysia. Lett. Appl. Microbiol. 46, 318–324. https://doi.org/10.1111/j.1472-765X.2007.02311.x